

# Mesenchymal Stem cells Ameliorate Diabetic Renocortical Changes In A Rat Model: Histological, Morphometrical And Biochemical Study

Original  
Article

Hekmat A. Ahmed- Sorour<sup>a</sup>, Mona Mohamed Abd-Elgalil<sup>b</sup>

<sup>a,b</sup>Histology Department, Faculty of Medicine for Girls, Al-Azhar University, Cairo, Egypt

## ABSTRACT

**Background:** Diabetic nephropathy (DN) is the most leading complication of renal disease. Mesenchymal stem cells (MSCs) therapy holds an excellent promise in the repair of injured tissues and organs. However, the precise effects of MSCs on renal cellular injury remain unclear.

**Objective:** This work was designed to evaluate the possible reno-therapeutic role of MSCs in experimental streptozotocin (STZ)-induced DN in adult female albino rat model.

**Materials and Methods:** Adult female albino rats were divided into three groups: Group I (control), Group II (diabetic group) and Group III (diabetic/MSCs treated group) where  $1 \times 10^6$  iron oxide-labeled MSCs was infused once in rat tail vein. Blood glucose levels and biochemical parameters of the kidney function such as serum creatinine (Cr), blood urea nitrogen (BUN) and uric acid were estimated. After 8 weeks, kidney specimens were processed for light and electron microscopic studies. Morphometric measurements and statistical analyses were done.

**Results:** STZ injection caused destructive glomerular, proximal (PCT) and distal (DCT) convoluted tubular changes within the renal tissue in the form of sloughed epithelium, vacuolated cytoplasm, pyknotic nuclei, congested blood vessels and mononuclear inflammatory cells infiltration that was supported by a significant increase in plasma concentrations of Cr, BUN and uric acid levels coupled to a significant elevation of Periodic-Acid-Schiff (PAS) reaction and increase in area percentage of collagen fibers. The ultrastructural assessment confirmed these distortions. In contrast, MSCs significantly corrected hyperglycemia and renal biochemical parameters with critical improvement in renal histopathological changes depicted previously.

**Conclusion:** MSC-based therapies may play a substantial therapeutic role in DN.

**Key Words:** Diabetic nephropathy, mesenchymal stem cells, Streptozotocin, diabetes mellitus

**Revised:** 21 August 2019, **Accepted:** 23 September 2019.

**Corresponding Author:** Mona Mohamed Abd-Elgalil, MD, Lecturer of Histology, Faculty of Medicine (Girls), Al-Azhar University, Cairo, Egypt, **Tel.:** (+2) 01090305671, **E-mail:** medicalmona2009@yahoo.com

ISSN:2536-9172, December 2019, Vol. 3, No. 2

## INTRODUCTION

One of the major complications of diabetes that might account for disability and end-stage renal deaths worldwide is diabetic nephropathy (DN). Terminal renal failure occurs within 7 years after the onset of renal disease and diabetic nephropathy<sup>[1]</sup>.

Streptozotocin induces diabetes type I by starting oxidative stress processes that destroy the Langerhans islets  $\beta$  cells. It suppresses and degenerates many of the enzymes involved in DNA synthesis<sup>[2]</sup>. Dyslipidemia<sup>[3]</sup>, renal inflammation and oxidative stress<sup>[4]</sup> also have a critical role in both initiation and progression of DN.

The risk for nephropathy with end-stage renal disease for type 1 (insulin-dependent) and type 2 (non-insulin-dependent) diabetic patients are not distinguishable<sup>[5]</sup>.

Prevention and treatment of diabetic nephropathy within the early stages and the slowing down of diabetic

nephropathy progression are among the most important topics for several ongoing research studies<sup>[1]</sup>.

To date, there is no remedy for DN. Drugs that decrease blood glucose, lower blood pressure, or inhibit the actions of the hormone angiotensin can delay, but not eliminate, the onset of DN. Hence, the improvement of novel restorative techniques that might particularly target DN is vital<sup>[6]</sup>.

Stem cells are undifferentiated cells that experience both self-renewal and differentiation into one or more cell types. Among stem cells, mesenchymal stem cells (MSCs) have several advantages for therapeutic use such as the ability to migrate to the destinations of tissue injury, strong immunosuppressive impacts<sup>[7]</sup> and better safety after infusion of allogeneic MSCs<sup>[8, 9]</sup>. The latter researchers described MSCs as potentially modern helpful therapeutic agents for the treatment of the complications of diabetes mellitus<sup>[9]</sup>.

The current study was designed to investigate the histological, biochemical and ultrastructural renal changes in experimentally induced diabetic nephropathy rats, and the possibility of MSCs injection to ameliorate these pathological changes.

## MATERIALS AND METHODS

Thirty-eight adult female Wistar albino rats aged 8 weeks and weighing  $140 \pm 20$  g were utilized in the current experiment. They were purchased from the Helwan Breeding farm, Egypt. Rats were bred in the animal house, Faculty of Medicine for Girls, Al-Azhar University, and kept up in an air-conditioned animal house in cages at room temperature ( $22\text{--}25^\circ\text{C}$ ) with specific pathogen-free conditions, and were subjected to a 12:12-h daylight/darkness. Rats were acclimatized, one week for adaptation before the beginning of the experiment and were allowed unlimited access to food and water throughout the experiment. All the ethical protocols for animal treatment were followed in accordance with the ethical procedures and guidelines of the Institutional Animal Care and Use Committee accepted by Faculty of Medicine for Girls, Al Azhar University, Egypt.

Rats were divided into 3 groups: Group I (Control group,  $n=18$ ) that was further subdivided equally into three subgroups (6 animals each): subgroup Ia: which served as a negative control received no treatment, subgroup Ib: included rats which received a single intraperitoneal injection of one ml. of 0.01 M citrate buffer (solvent of streptozotocin) after being starved for 16 hours, subgroup Ic: included animals that received an equivalent volume of phosphate buffer saline in tail vein, diabetic group ( $n=20$ ) in which diabetes was induced by a single intraperitoneal injection of streptozotocin (STZ) 60 mg/kg body weight dissolved immediately before administration in freshly prepared 0.01 M citrate buffer (pH 4.5) after being starved for 16 hours to induce diabetes<sup>[10]</sup>. STZ was purchased from Sigma Company, St.Louis, Mo, USA. One droplet of blood was placed on a glucose test strip and read using a glucometer (SD Code free blood glucose monitoring system, SD Biosensor, INC., Korea). Diabetes was defined as a fasting blood glucose reading of  $>200$  mg/dl on the 3rd day after STZ injection which was considered the first day of the experiment<sup>[11]</sup>. The diabetic rats were selected and subdivided equally into; Diabetic nephropathy group (GII): 10 Diabetic rats received nothing following STZ throughout the whole duration of the study (8 weeks). Diabetic/ MSCs group (GIII): 10 diabetic rats injected once with  $1 \times 10^6$  cultured and labeled bone MSCs suspension in 1ml phosphate buffer saline (PBS) / kg body weight /rat in the tail vein<sup>[12]</sup>.

BM-derived MSCs were prepared in the Clinical Pathology Department, Kasr Al-Ainy Faculty of Medicine, according to the method of some investigators<sup>[13, 14]</sup>.

The samples were cultured and labeling of MSCs was performed. MSCs were suspended in phosphate buffer saline (PBS). Labeled cells with ferumoxides were histologically assessed using Prussian blue stain<sup>[15, 16]</sup>.

The treatments were continued for 8 weeks. The animals of all groups were weighed individually at the beginning of the experiment and at the end just before collecting samples.

At the end of the experiment (8 weeks post STZ injection), blood was collected immediately retro-orbitally in sterile tubes using a heparinized capillary tube under ether anesthesia<sup>[17]</sup> for blood glucose, blood urea nitrogen (BUN), serum creatinine (Cr) and uric acid estimation enzymatically using commercially available kits (Bioclin, Santa Coloma, Spain). The serum levels of (BUN), (Cr) and uric acid, were estimated by the conventional colorimetric method using QuantiChrom™ assay kits according to the manufacturer's instruction (BioAssay Systems, CA 94545, USA)<sup>[12]</sup>.

Kidney samples were collected, fixed in 10% formalin for 72 hours, and processed to obtain paraffin 5 $\mu$ m thick sections. Sections were stained with Hematoxylin and Eosin (H&E) for routine histological examination to study the general structure, Masson's trichrome stain, for staining the collagen fibers, Periodic acid Schiff's (PAS) technique for detection of polysaccharides in the renal tissue<sup>[18]</sup> and Perl's Prussian blue (PPB) staining technique counterstained by eosin, for detection of iron oxide labeled therapeutic stem cells<sup>[15, 16]</sup>.

### Electron microscopic study

Electron microscopic preparation was used to detect the renal ultrastructure changes and changes in the glomerular basement membrane thickness. Small pieces (1 mm<sup>3</sup> thickness) of renal cortex of each animal were fixed immediately in 2.5% glutaraldehyde for 24h, placed in phosphate buffer for 24 hours, post-fixed in 1% osmium tetroxide, dehydrated and embedded in resin, followed by semi-thin sections stained with toluidine blue and ultrathin sections were stained with uranyl acetate and lead citrate<sup>[19]</sup>. Sections were examined by an electron microscope JEOL, TEM 1010 (Tokyo, Japan), at the electron microscopic unit of the Regional Center for Mycology and Biotechnology (RCMB), Al Azhar University.

### Quantitative, Morphometric and Statistical Studies:

The body weight, blood glucose level, kidney function tests were measured in all the groups. Different quantitative morphometric parameters were measured in renal sections using the ImageJ software, version 1.46. The area percentage of the collagen fibers of Masson's trichrome stained sections at X400 magnification was measured in a standard frame

of 7104.45 $\mu$ m<sup>2</sup>. In each chosen field, the area of collagen was measured by adjusting the colour threshold and then the red-stained area limited to threshold was selected while excluding the background then the mean values were calculated<sup>[20]</sup>. In addition, the mean optical density of PAS in PAS stained sections at X400 magnification was measured in a standard frame of 6638.84 $\mu$ m<sup>2</sup><sup>[21]</sup>. 10 non-overlapping fields from five sections of each rat in each group (n=10), were chosen from the parameter measured and analyzed morphometrically. Finally, the mean thickness of the glomerular basement membrane (GBM) was measured in 10 non-overlapping fields from electron microscopic sections in different groups at 15000 magnification (3 fields in each section)<sup>[22]</sup>, using the microscope image analyzer software at the Regional Center for Mycology and Biotechnology(RCMB), Al-Azhar University, Cairo, Egypt.

All data were statistically expressed as means  $\pm$  SD and compared using the one-way analysis of variance (ANOVA) followed by Tukey's post hoc test. The level of probability (*P-value*) < 0.05 is used as the criterion of significance. Statistical analysis was performed using the Statistical Package for the Social Sciences, Version 22 for Windows (California, USA)<sup>[23]</sup>.

## RESULTS

---

### ***Histological results:***

Examination of sections from the three control subgroups (1a, 1b & 1c) showed more or less similar structure with no observed changes between them.

### ***Hematoxylin and Eosin (H&E) stain (Figs.1a-1h)***

H&E stained sections from the control group revealed the normal histological architecture of renal parenchyma with normal appearance of Malpighian renal corpuscles and renal tubules that incorporate proximal convoluted tubules (PCTs), distal convoluted tubules (DCTs) and collecting tubules with minimal interstitium (Fig.1a).

Malpighian renal corpuscles demonstrated a typical glomerular structure composed of a glomerular tuft of interconnected blood capillaries surrounded by visceral and parietal layers of Bowman's capsule limited narrow urinary space (Bowman's space) in between. The outer parietal layer lined with a simple squamous epithelium whereas the inner visceral layer enveloped the glomerular tuft of capillaries with cells containing deeply stained oval or flattened nuclei (Fig.1a).

The PCTs constituted the main bulk of the cortex with a characteristic narrow lumen occupied by prominent brush border and were lined by simple cuboidal epithelium with eosinophilic cytoplasm, centrally located spherical vesicular nuclei and prominent nucleoli (Fig.1a).

DCTs were less commonly observed in the renal cortex, they were wider than PCTs and lacked a brush border and lined by more cubical cells with a faint acidophilic cytoplasm and central spherical nuclei bulging into the lumen. Peritubular capillaries appeared separating the convoluted tubules (Fig.1a).

The renal medulla revealed wider thin-walled collecting tubules lined by low cubical cells and separated by minimum interstitial tissue (Fig.1b).

Inversely, an examination of the H&E stained renal sections of the Diabetic nephropathy group (GII) revealed areas of apparent aggravated glomerular, tubular and interstitial histological alterations in the form of expanded lobulated glomeruli contained dilated congested intraglomerular blood capillaries with narrowed or even obliterated Bowman's space. The glomerular cells had small darkly stained nuclei (Figs.1c, 1d & 1e).

Sever vacuolar degeneration of the epithelial lining of multiple cortical proximal and distal convoluted tubules that appeared dilated with hydropic degeneration and apoptotic changes in the form of vacuolated cytoplasm and darkly stained small shrunken pyknotic nuclei with chromatin condensation and loss of the regular cellular arrangement. In addition, loss of the apical brush border in many degenerated proximal convoluted tubules was noticed. Cell desquamation or shedding of the epithelial lining cells, intraluminal homogenous acidophilic hyaline casts (intraluminal casts) and cellular debris were also detected (Figs.1c, 1d & 1e).

Sections in the renal medulla of diabetic rats showed vacuolated cytoplasm exhibiting flattened dark pyknotic nuclei in the epithelial cells lining of multiple collecting tubules. Desquamated nuclei were occasionally detected in their lumen. Besides, dilated congested blood peritubular capillaries, mononuclear inflammatory cells infiltration, extravasation of red blood corpuscles and areas of haemorrhage were also noticed within the deformed interstitial tissue between the renal tubules (Fig.1f).

Diabetic/ MSCs group (GIII) revealed prominent structural improvement when compared to the diabetic-only group and almost regaining of the renal histological architecture nearly as was seen in the control group. Also, no glomerular degeneration was observed. Most of the renal tubules appeared intact without vacuolar degeneration. No cellular infiltration and no congested capillaries could be noticed (Figs.1g & 1h).

## Fig.1 Hematoxylin and Eosin (H&E)

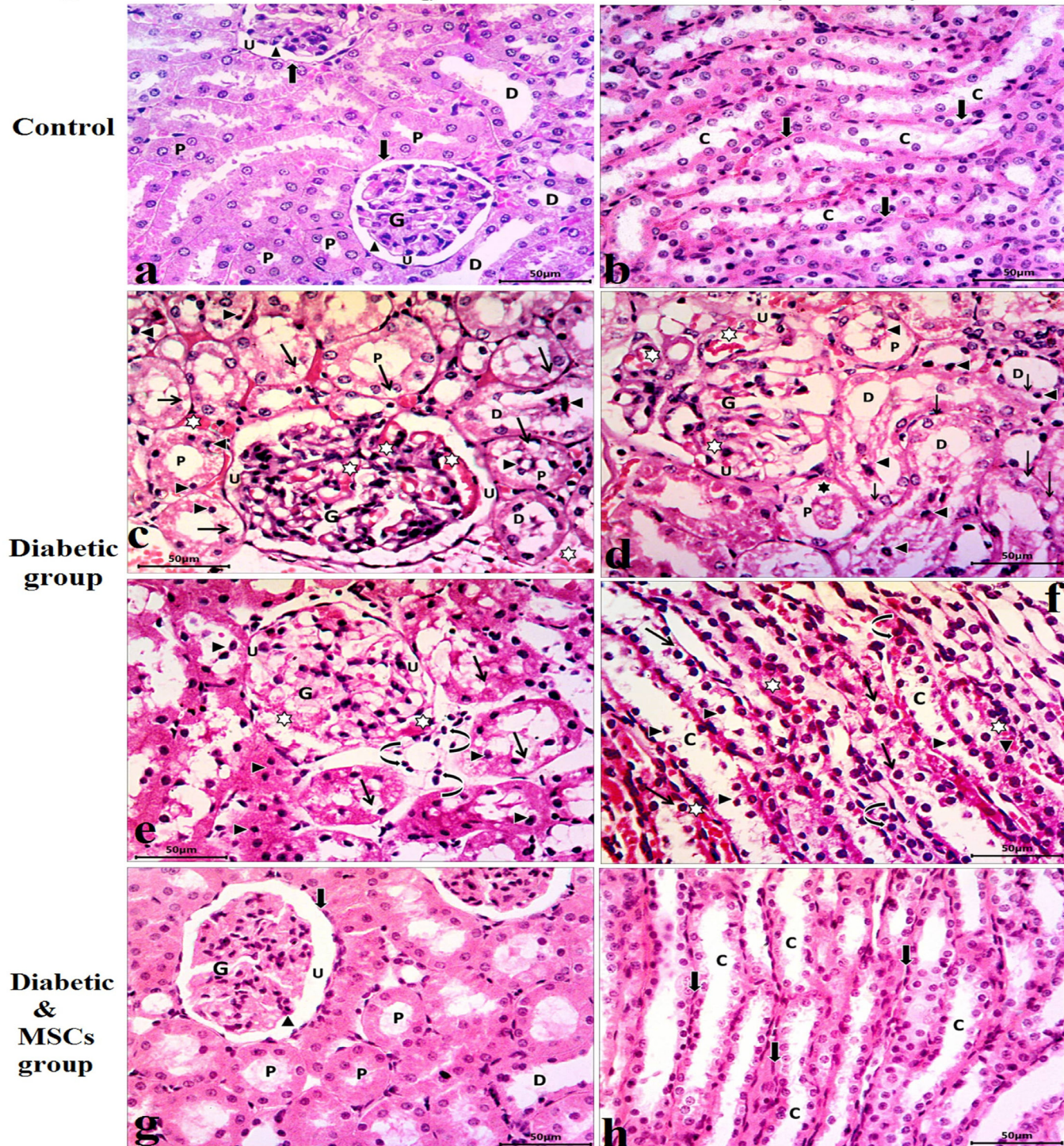


**Fig 1:** Photomicrographs of the renal tissue from the experimental groups: control (a-b), (a) Normal renal architecture consists of a glomerulus (G), contained a tuft of capillaries surrounded by parietal simple squamous epithelial (black arrow) and visceral (arrowhead) layers of Bowman's capsule. PCTs (P) are lined by pyramidal cells with central rounded vesicular nuclei. DCTs (D) have a wider lumen, more cubical cells and rounded nuclei bulging into the lumen. (b) Low cubical cells of collecting tubules (C) separated by minimum interstitium (black arrow) in the renal medulla. Diabetic group (c-f), demonstrating: Congestion of intraglomerular (G) and intertubular blood capillaries (white stars). Expanded lobulated glomerulus has small darkly stained nuclei and narrow Bowman's space (U). Distorted proximal (P) and distal (D) convoluted tubular epithelial cells have vacuolated cytoplasm (arrows). Exfoliated cells with darkly stained pyknotic nuclei (arrowhead). Homogenous intratubular acidophilic casts in some tubules (black star). Interstitial mononuclear Inflammatory cell infiltration (curved arrow) is noticed surrounding the destructed tubules. Peritubular congested blood capillaries in between collecting tubules (white stars) within the renal medulla along with exfoliated tubular epithelial cells have dark-stained pyknotic nuclei (arrowhead). Diabetic/MSCs group (g-h): show a potentially alleviated renal histoarchitecture, normal renal corpuscles, glomeruli (G) surrounded by parietal (black arrow) and visceral (arrowhead) layers of Bowman's capsule, regular urinary space in between (U). Narrow PCTs (P) and wide DCTs (D) (H&E X400, Scale bar; 50µm)

**Masson's trichrome stain (Figs.2a-2f):**

Masson's trichrome stained sections of the control group (GI) demonstrated fine strands of collagen fibers which were concentrated mainly around the Bowman's capsule, among the glomerular capillaries (Fig.2a) and scanty fine scattered collagen fibers within the narrow interstitial tissues between renal tubules (Fig.2b).

Sections of the diabetic nephropathy group (GII) revealed obviously increased density and distribution of

the collagen fibers around the glomeruli, intraglomerular around the glomerular capillaries (Fig.2c) and also peritubular in the interstitium compared with the control group (Fig.2d).

Diabetic/ MSCs group (GIII) sections revealed a nearly normal distribution of collagenous fibers around renal corpuscles (Fig.2e) and at the boundary of renal tubules in the interstitium that appeared quite similar to the control (Fig.2f).

**Fig.2 Masson's trichrome stain**

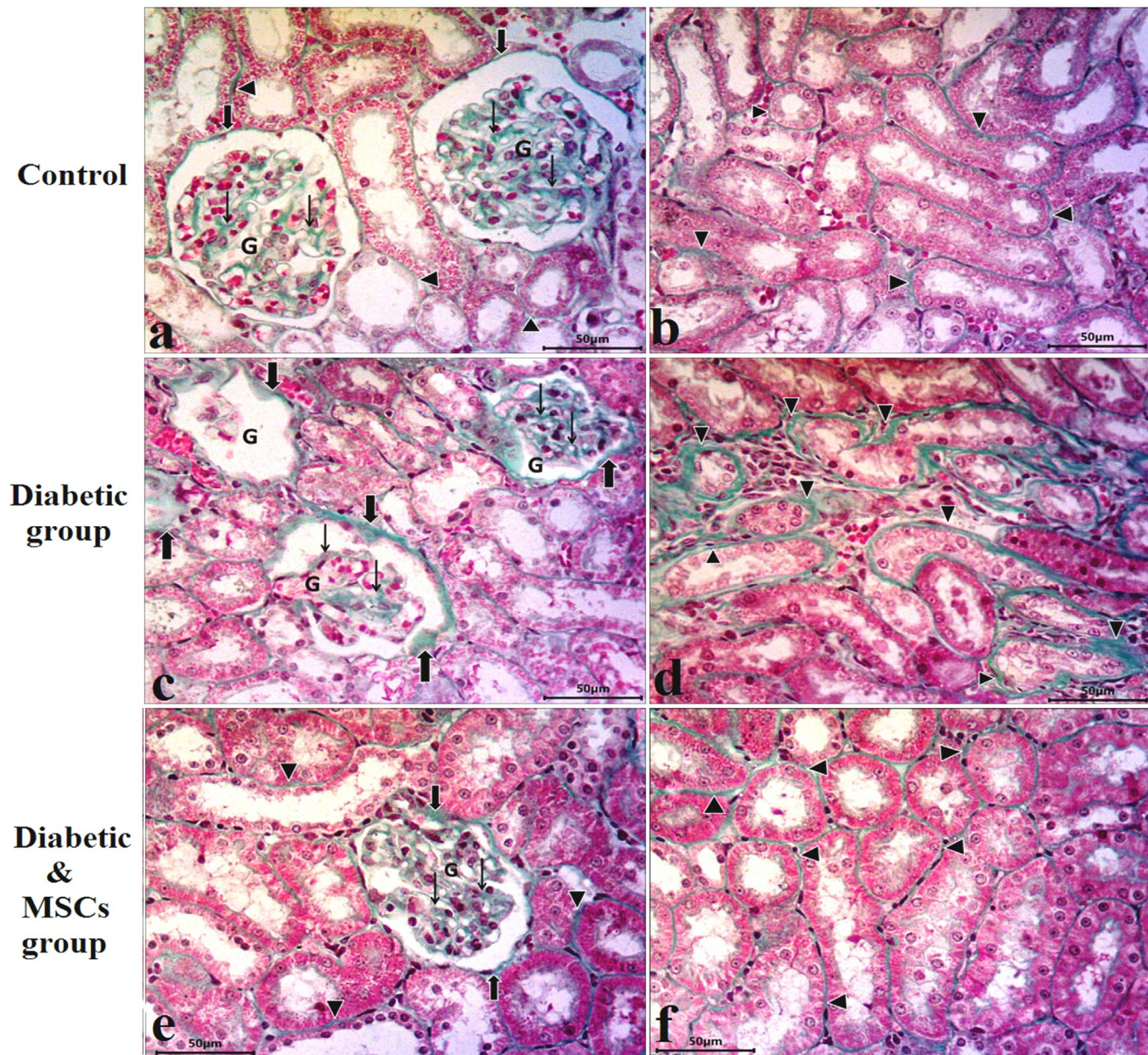


**Fig. 2:** Photomicrographs of the renal tissue from the experimental groups: control (a-b): (a) Normal distribution of fine collagen fibers around the Bowman's capsule (thick arrows), intraglomerular (G) between the glomerular tuft of capillaries (thin arrows) and scanty fine collagen fibers in the interstitium in-between the renal tubules (arrowhead). Diabetic group (c-d): showing increase deposition of collagen fibers in the intraglomerular (thin arrows) tissue among the distorted glomeruli (G), in the pericapsular (thick arrows) areas around the renal corpuscles and the peritubular areas (arrowhead) in the interstitium. Diabetic/MSCs group (e-f): show a normal distribution of fine collagen fibers among the glomerular capillaries (thin arrow), pericapsular (thick arrows) and scanty fine scattered collagen fibers in the interstitium (arrowhead). (Masson's trichrome X 400, Scale bar; 50µm).

**Periodic acid Schiff technique (Figs.3a-3c):**

PAS stained sections of the control group (GI) showed intraglomerular PAS +ve materials with strong PAS reaction at the well-circumscribed thin, regular capsular, glomerular basement membranes and tubular membranes that were seen investing the renal tubules in addition to strong PAS reaction at the luminal intact brush border of almost all proximal convoluted tubules. Weak PAS-positive reaction at the apical tubular cells of the distal convoluted tubules was also noticed (Fig.3a).

The untreated diabetic nephropathy group (GII), in comparison with the control group, showed an increase in the dense staining intraglomerular mesangial matrix content evidenced by the strong intraglomerular PAS-

positive reaction, thickened basement membranes of the parietal layer of Bowman's capsule, basement membranes of glomerular capillaries and basement membranes of some renal tubules which were densely stained. Marked dense PAS-positive intracytoplasmic granules were seen in the cytoplasm of the PCTs (Armani-Ebstein cells). Inversely, faint or even PAS negative reaction at the disintegrated brush borders of these PCTs was also observed (Fig.3b).

In diabetic/ MSCs group (GIII) sections the mucopolysaccharide content was nearly similar to the control. MSCs treated group showed normal intraglomerular and tubular PAS-positive reaction and at the luminal continuous brush border of the proximal convoluted tubules closely similar to that of the control group (Fig.3c).

**Fig.3 Periodic acid Schiff's (PAS) reaction**

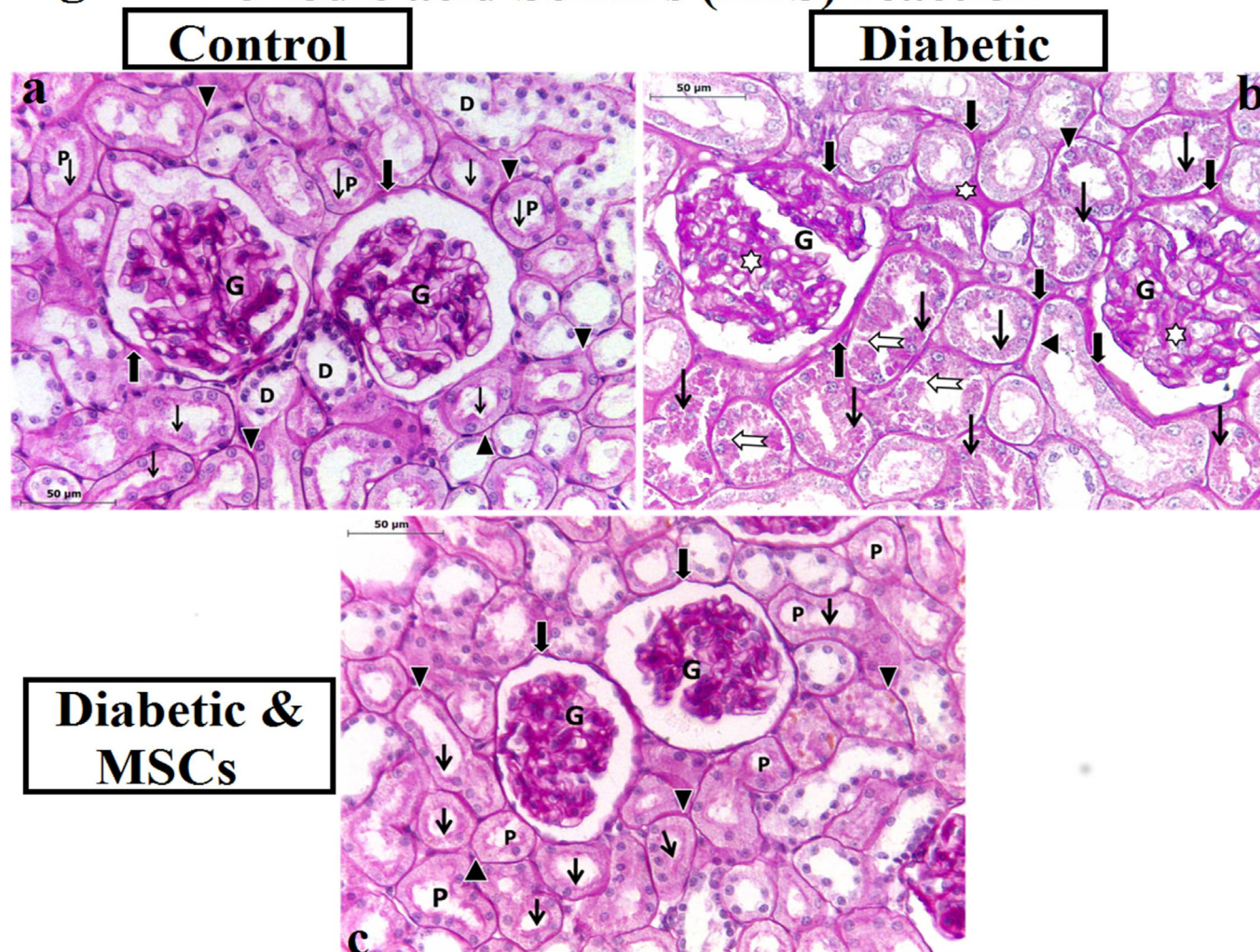


**Fig. 3:** Photomicrographs of the renal tissue from the experimental groups: control (a) showing: strong PAS-positive reaction in the glomeruli (G), at regular capsular (thick arrow), tubular (arrowhead) basement membranes and the intact apical brush borders (thin arrow) of the PCTs (P). Notice, tubular cells of the DCTs (D) have weak PAS-positive reactions at their apical borders. Diabetic group (b) showing: mesangial matrix expansion with strong dense PAS-positive staining intraglomerular mesangial matrix (white stars) within degenerated lobulated glomeruli (G). Thickened basement membranes of the parietal layer of Bowman's capsule and basement membranes of some renal tubules (thick black arrows). Notice, focal loss of PAS reaction at the interrupted apical brush borders (bifid white arrows) and obvious dense PAS-positive intracytoplasmic granules (thin black arrows) of the tubular epithelial cells (Armani-Ebstein cells) of the PCTs. Focal areas of the detached epithelial cells from their underlying basal lamina (arrowheads) are also detected. Diabetic/MSCs group (c): showing high restoration of the capsular (thick arrow), glomerular (G) and tubular (arrowhead) strong PAS-positive reaction and at the intact apical brush borders (thin arrow) of the PCTs (P) (PAS reaction x 400, Scale bar; 50µm).

**Prussian blue stain (Figs.4a-4c):**

Prussian blue-stained sections of the control group (GI) showed negative staining with Prussian blue counterstained with neutral red among Malpighian renal corpuscles and cortical tubules (Fig.4a). No changes had been observed between the different control subgroups.

Similarly, sections of the diabetic group (GII), revealed negative staining with Prussian blue counterstained with

neutral red among the previously mentioned structures (Fig.4b).

Sections of diabetic /MSCs group (GIII) revealed multiple spindles, polygonal and some cuboidal Prussian blue positive (+ve) cells at the glomeruli, in the Bowman's space and at the epithelial lining of the cortical tubules (Fig.4c).

**Fig.4** Perls Prussian blue staining technique

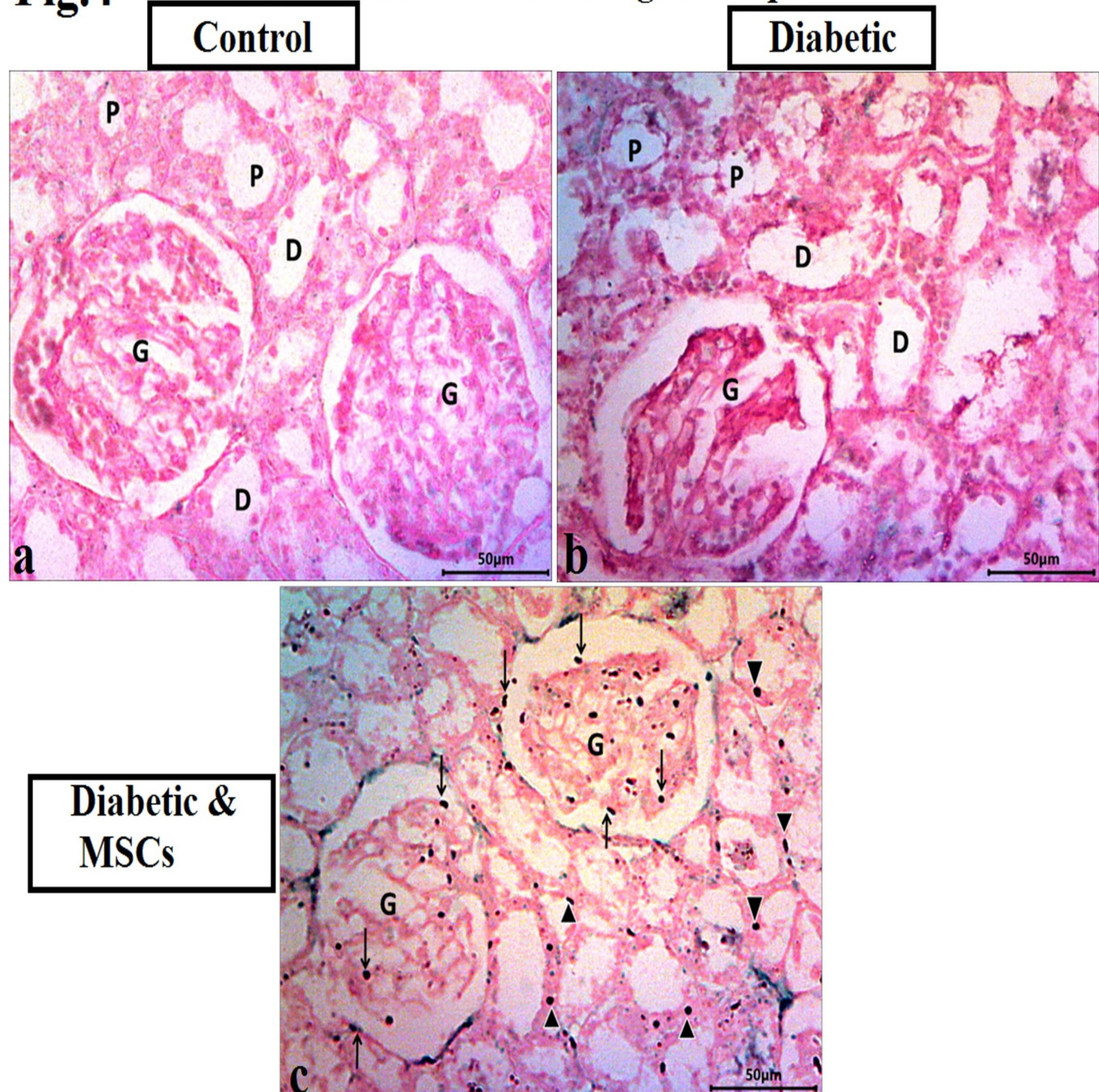


**Fig. 4:** Photomicrographs of the renal tissue from the experimental groups: control (a) showing: negative staining with Prussian blue and Neutral red in (G), PCTs (P) and DCTs (D). Diabetic group (b): showing negative staining with Prussian blue and Neutral red in the distorted (G), degenerated PCTs (P) and DCTs (D). Diabetic/MSCs group (c): showing multiple Prussian blue +ve spindle and cubical cells (arrows) at the glomeruli (G), and at the epithelial lining of the renocortical tubules (arrowheads). (Prussian blue, x400 Scale bar; 50µm).

**Semithin renal sections examination (Figs.5a-5c):**

A section in the renal cortex of a control rat kidney showed normal glomerular capillaries. The proximal convoluted tubules had rounded vesicular nuclei variable in position with a distinct brush border. The renal corpuscle was lined by a parietal layer of Bowman's capsule. The podocytes which line the visceral layer, embrace the glomerular capillaries contained red blood corpuscles and the intraglomerular mesangial cells (Fig.5a).

The diabetic group (GII) revealed distortion of the glomerular structure. Desquamated cells with loss of the

cellular architecture of the proximal convoluted tubules that had vacuolated cytoplasm with dense and distorted pyknotic nuclei. Some cells still have vesicular nuclei (Fig.5b).

In diabetic/MSCs treated rats (GIII), there was almost restoration of glomerular and tubular architecture. There was a notable structural improvement in the form of preservation of the brush border and vesicular nuclei in both the proximal and distal tubules. Besides, the renal corpuscles preserved their normal architecture (Fig.5c).

**Fig.5 Semithin sections of all experimental groups**

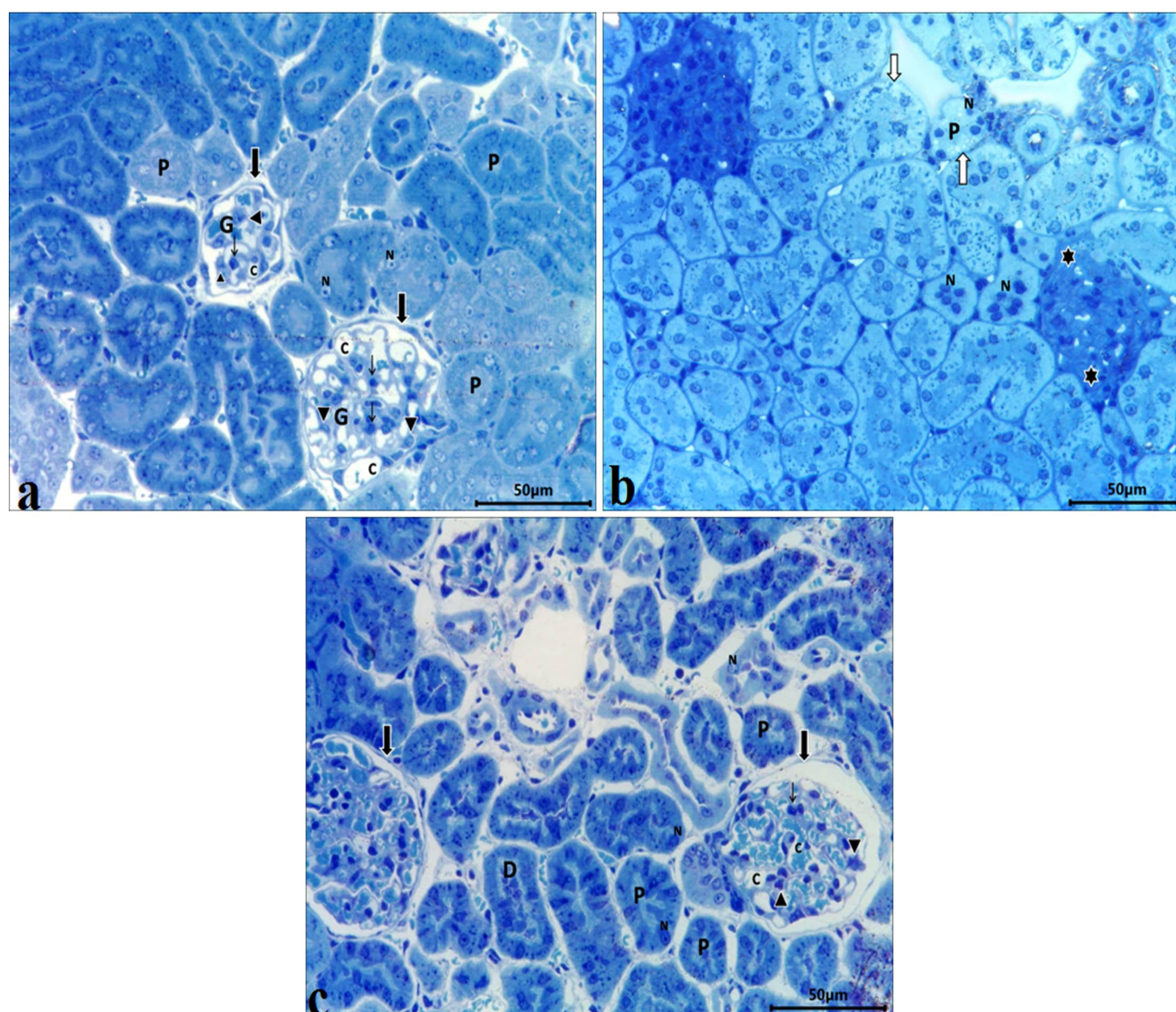


**Fig. 5:** Photomicrographs of the semithin sections of renocortical tissue from the experimental groups, showing: control (a) a parietal layer of Bowman's capsule (thick arrow). The podocytes (arrowhead) embrace the glomerular capillaries (C) and mesangial cells (thin arrows). The PCTs (P) show vesicular nuclei (N) and a distinct brush border. Diabetic group (b): showing: distortion of the glomerular structure (stars), desquamated cells of the PCTs (P) have vacuolated cytoplasm (white arrows) with dense and distorted pyknotic nuclei (N).Some cells still have vesicular nuclei. Diabetic/MSCs group (c): showing a preserved parietal layer of Bowman's capsule (thick arrow), podocytes (arrowhead) embrace the glomerular capillaries (C) and mesangial cells (thin arrows). There is a notable restoration of the brush border and the vesicular nuclei (N) in both PCTs (P) and DCTs (D). ( Toluidine blue x400 Scale bar; 50µm).

**Ultrastructural examination :**

The ultrastructural examination of the control group (GI) revealed the renal filtration barrier interposed between the fenestrated endothelial cells of glomerular capillaries and the pores (filtration slits) between the secondary processes (series of pedicles) of the podocyte. The regularly thickened glomerular basement membrane appeared in the form of a central electron-dense layer and bilateral electron-lucent layers. The podocytes were oval with flattened euochromatic nuclei and electron-dense cytoplasm, long primary processes, which branched to give

secondary processes. The latter gave rise to feet processes, which were separated by the narrow slits membrane. Podocytes and cytoplasmic extensions, infiltration slits were evenly distributed and associated with the capillary surfaces not covered by mesangial cells. Mesangial cells were evident and the amorphous mesangial matrix appeared in many places continuous with the basement membrane. The matrix supported capillary loops where podocytes were lacking. Some mesangial processes appeared to pass into the capillary lumen where they may help endocytose adherent protein aggregates (Fig.6).

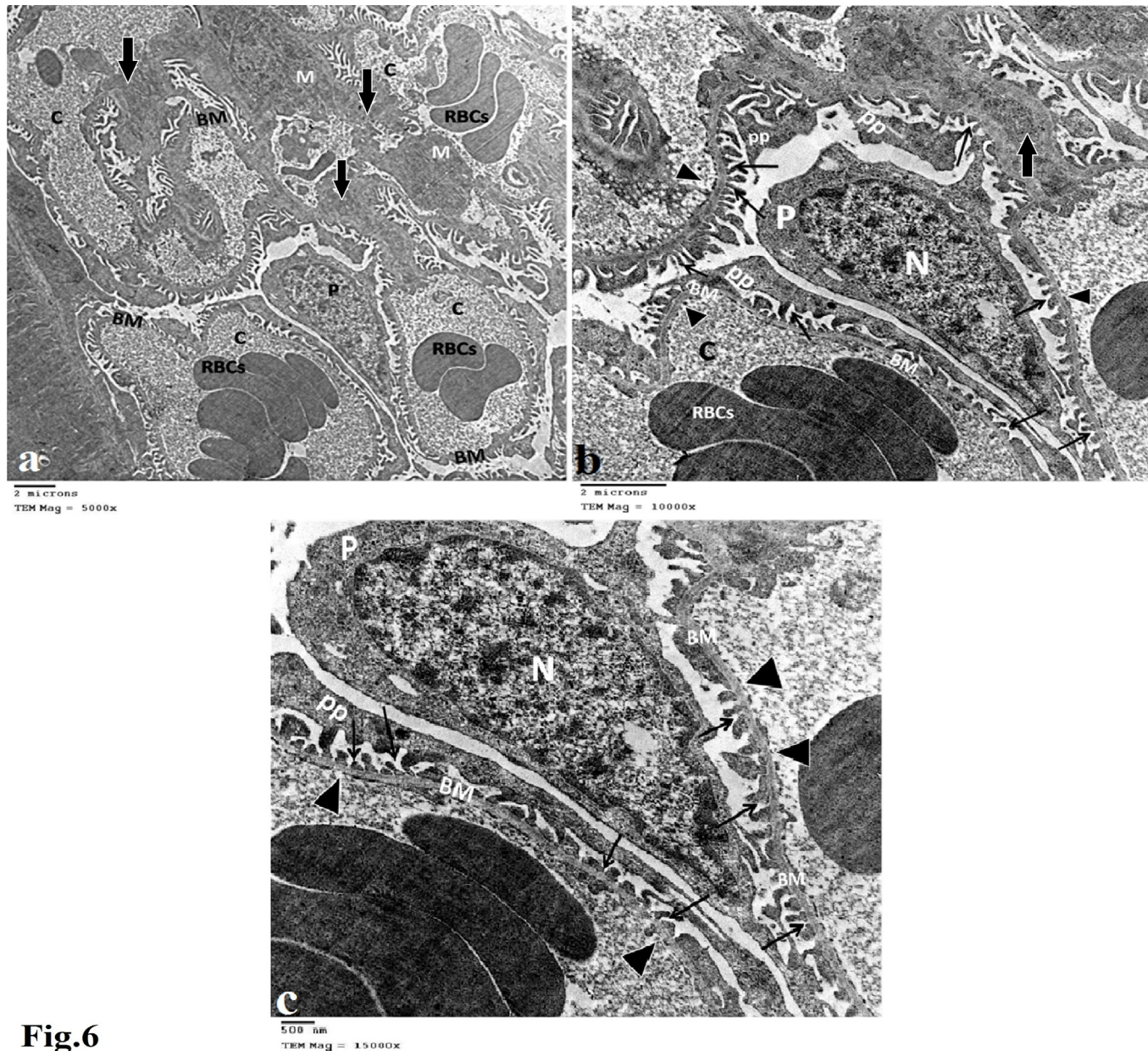


**Fig.6**

**Fig. 6:** Transmission electron photomicrograph of a section in the renal glomerulus from a control rat showing : (a) a glomerular tuft of capillaries (C) contain red blood corpuscles (RBCs) and covered by intact podocyte (P). Notice, mesangial cells (M) with a little amorphous mesangial matrix (arrows). (b) Amorphous mesangial matrix (thick arrow) appears continuous with the capillaries basement membrane (BM). (b,c) The podocyte (P) is an oval cell with flattened euochromatic nucleus (N), electron-dense cytoplasm, long primary processes (PP) and filtration slits between its foot processes (thin arrows) on the glomerular basement membrane. (c) Regular thickness of the glomerular basement membrane (BM) with the distinct 3 layers (central electron-dense layer with bilateral electro-lucent layers) appears surrounded with podocyte pedicles (thin arrows) on one side and fenestrated endothelium (arrowhead) of the glomerular capillary on the other side [a, X5000; b, X10000 &c, X15000].

The PCTs had a normal structure lined with cuboidal cells contained large rounded euchromatic nuclei with peripherally arranged heterochromatin, and prominent nucleoli. Abundant elongated basally located mitochondria with intact cristae and electron-dense internal matrices, arranged parallel to the vertical axis of the cell were seen in between basal infoldings and also there were extensive

lateral wall interdigitations. The apical surface of the cells had closely packed regular microvilli forming the brush border. The cytoplasm contained dense bodies, most probably proteins, lysosomes, and some apical vacuoles and pinocytotic vesicles. The basement membrane is regular and of even thickness (Fig.7).

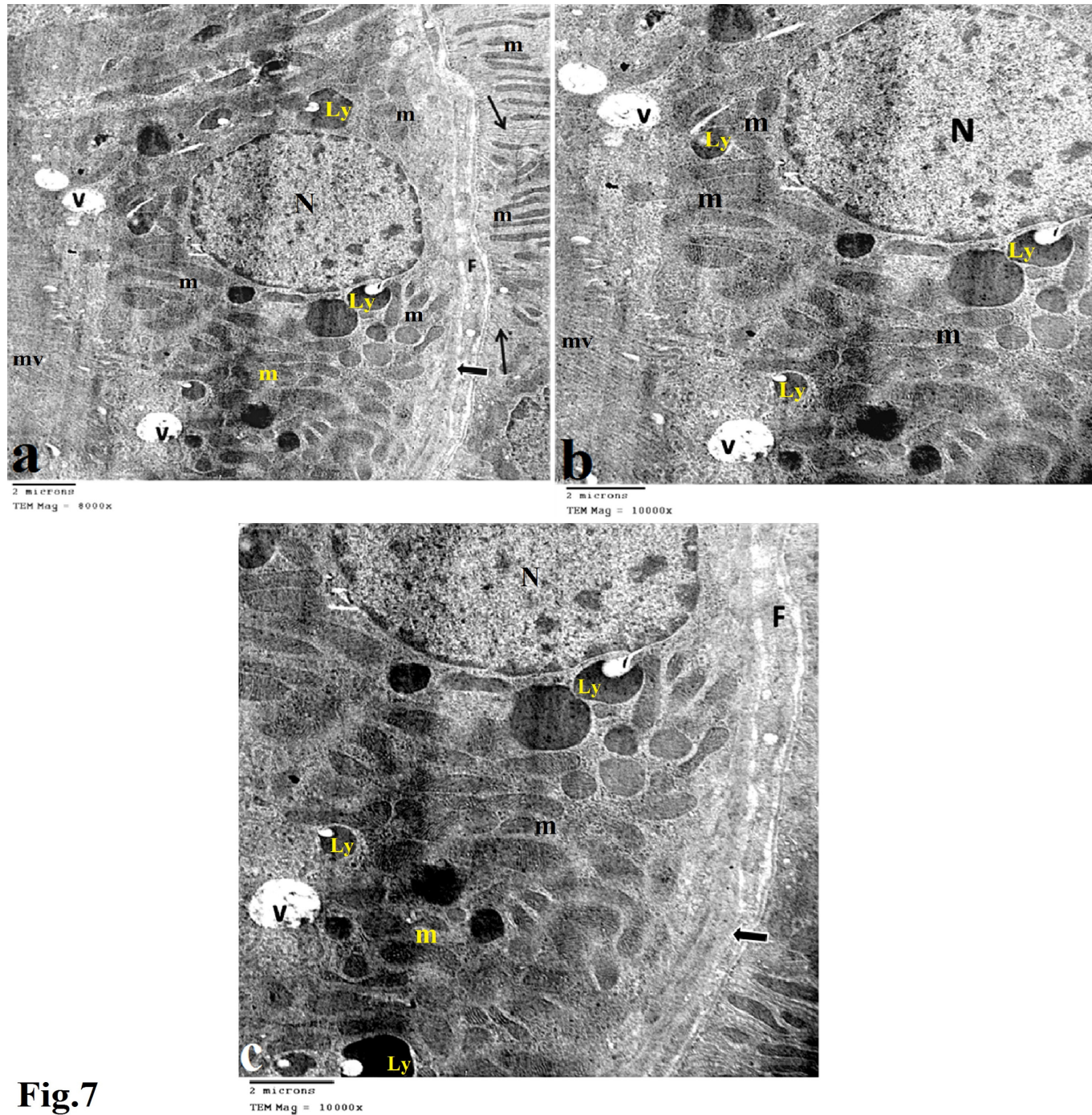


**Fig.7**

**Fig. 7:** TEM of the lining cells of PCT in the renal cortex from a control rat (a-c) showing: cuboidal cell has a large rounded euchromatic nucleus (N), multiple elongated radially arranged mitochondria (m) between basal infolding (thin arrows), apical vacuoles (V), dense bodies, lysosomes (Ly), mitochondria (m) and numerous apical microvilli (mv). (b,c) mitochondria (m) appear with intact cristae and electron-dense internal matrices. (a,c) the cells rest on thin regular basal lamina (thick arrow). Between the basement membranes of the tubules, there is an extension of a fibroblast (F). [a, X8000; b, X10000 &c, X10000].

The DCTs showed intact low cuboidal cells with open face nuclei, The apical cellular membrane having few short microvilli compared with the proximal tubules, numerous

regular basal infoldings and elongated intact mitochondria with almost intact cristae in between. Cells possessed many small pinocytotic vesicles (Fig.8).

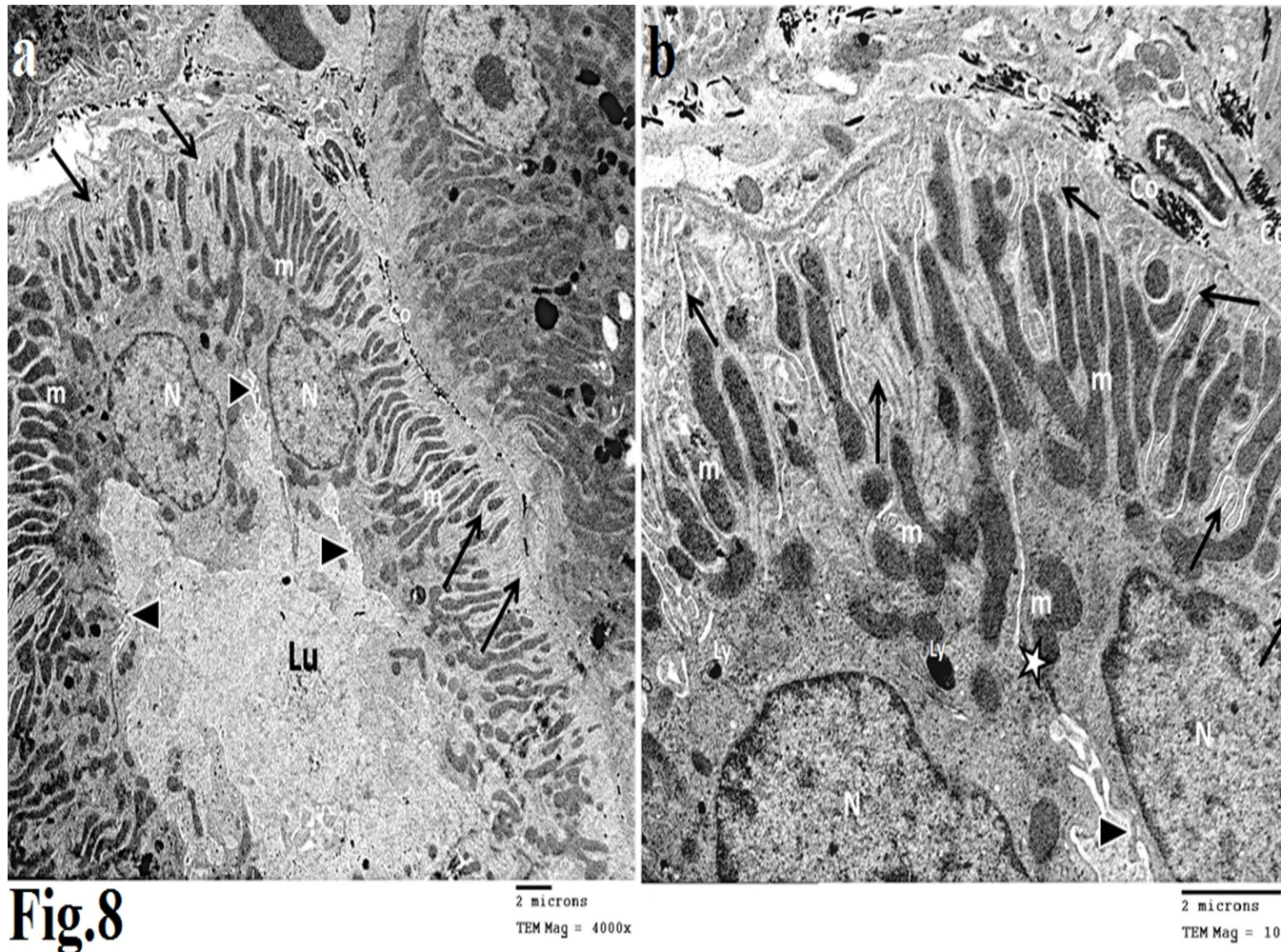


**Fig. 8:** TEM of a section in the renal cortex from a control rat showing: (a) A normal distal convoluted tubule appears lined with cuboidal cells bulge into the lumen (Lu) and large spherical, euchromatic, apically located nuclei (N) with normal peripheral chromatin distribution. (b) A higher magnification figure showing: extensive basal infoldings of the plasma membrane (thin arrows) with numerous elongated basally arranged mitochondria (m) have intact cristae and electron-dense internal matrices. Lysosomes (Ly) and poorly developed blunt apical microvilli (arrowhead). Apical ends of adjacent cells are sealed with desmosome (white star). Cut section of collagen fibers (Co) in different directions and flattened fibroblasts (F) are also observed. [a, X4000 & b, X10000].

The most apparent finding in the glomerulus of the untreated diabetic group (GII) was a completely developed diabetic nodular lesion glomerulosclerosis which destroyed the normal architecture of glomerular tufts, degeneration of the parietal layer of the Bowman's capsule where the degenerated epithelial cells had small shrunken heterochromatic pyknotic nuclei and diffuse thickening of the capsular basement membrane. Subepithelial hyalinosis shown as empty large irregular areas beneath the basal

lamina with an expansion of electron-dense intraglomerular mesangial matrix invaded most of the whole glomerulus and encroached on the capsular wall caused sclerotic nodules and apoptosis of the podocytes. Cellularity was decreased in the central area of the glomeruli with disproportional cell distribution. Pericapsular heavy clusters of collagen fibers in different directions with regular periodicity and flattened fibroblasts were also observed (Fig.9).

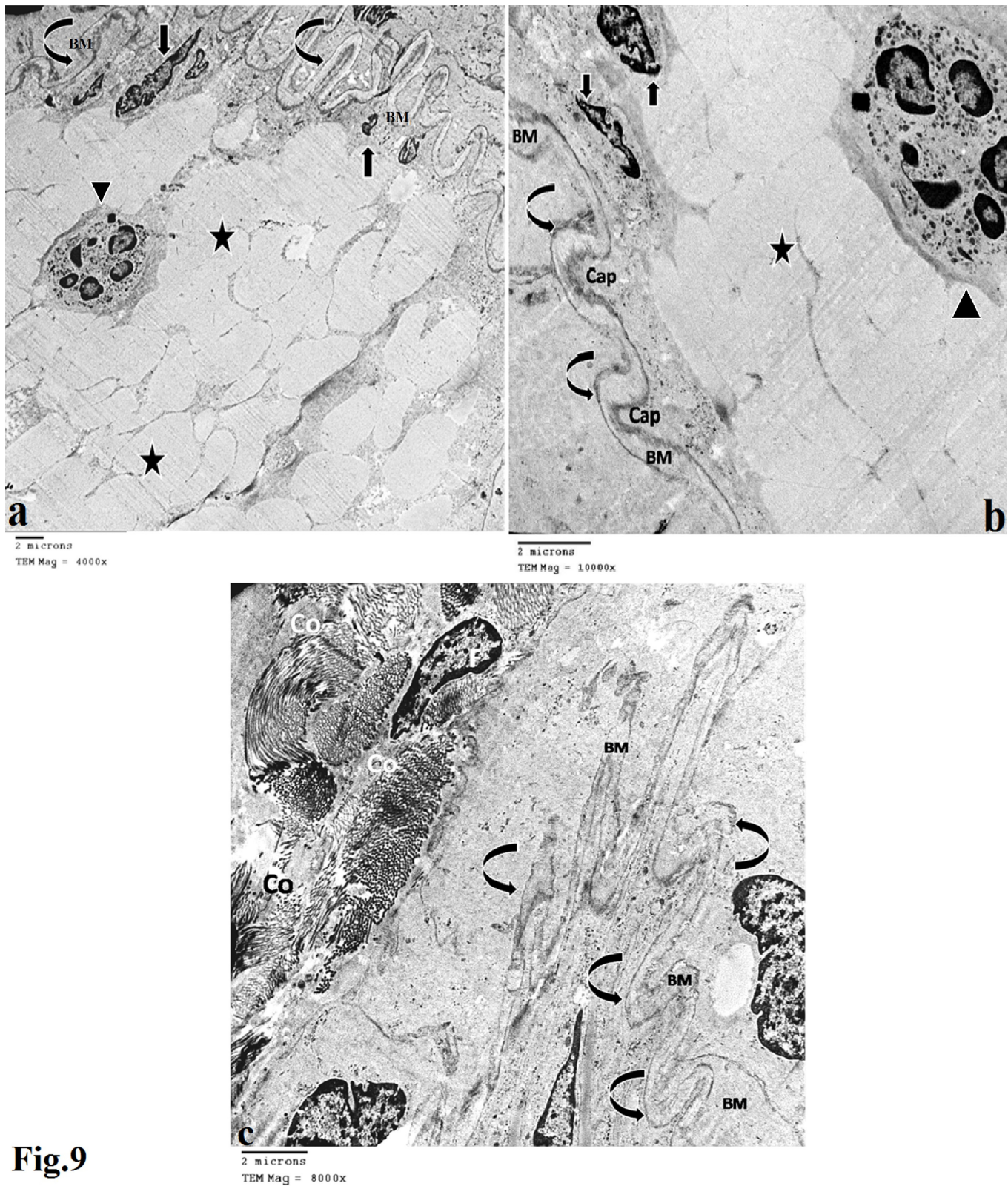


**Fig.9**

**Fig. 9:** TEM of a section in the renal glomerulus from the diabetic group showing: (a,b) Nodular lesion in diabetic glomerulosclerosis. Subepithelial hyalinosis with an expansion of intraglomerular electron-dense mesangial matrix (star) invades most of the whole glomerulus and encroaches on the capsular wall (Cap). Degenerated epithelial cells in the peripheral area have small shrunken heterochromatic pyknotic nuclei (arrows). Apparent diffuse thickening (curved arrows) of the capsular basement membrane (BM). Notice, intraglomerular neutrophil (arrowhead) with a segmented nucleus. (c) Pericapsular heavy clusters of collagen fibers (Co) cut in different directions with regular periodicity and flattened fibroblast (F) are also observed close to the diffusely thickened (curved arrows) capsular basement membrane (BM). [a, X4000; b, X10000 &c, X8000].

In the other regions of the renal glomeruli secondary to STZ, there was diffuse lesions glomerulosclerosis exhibited global mesangial expansion that was determined both by mesangial cell hypertrophy which had round cellular shape with lesser small cytoplasmic processes and accumulation of mesangial matrix. Collagen fibrils were expanded in the central stalk of glomerular tufts. Deformed

podocytes with broadening, widening and effacement of most of their feet processes. Destruction and loss of fenestrations of endothelial cells of the capillaries without the destruction of the normal architecture of glomerular tufts were detected. Diffuse thickening of the glomerular basement membrane with indistinct and ill-defined layers as compared with that of the control group (Fig.10).

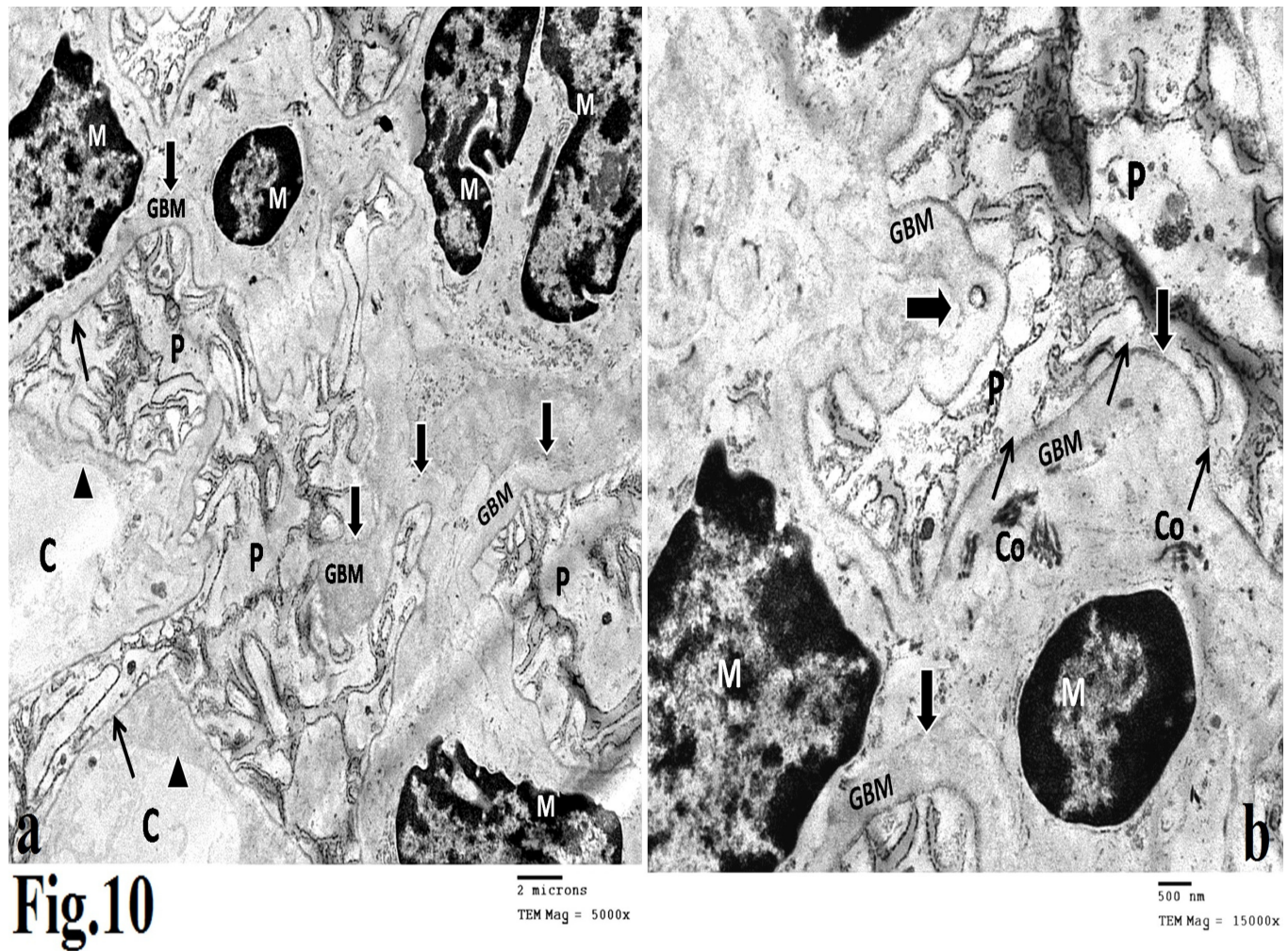


**Fig.10**

**Fig. 10:** TEM of a section in the renal glomerulus from a diabetic rat showing: (a-b) Apparent diffuse thickening (thick arrows) of the glomerular basement membrane (GBM) compared with the control and deformed mesangial cells (M) have heterochromatic distorted nuclei with expanded mesangium. Notice, loss of fenestration of endothelial cells (arrowheads) of the glomerular capillaries (C). Broadening and segmental effacement of the overlying foot process (thin arrows) of the podocytes (P) is seen. Notice, non-specific mesangial collagen fibrils (Co) in different directions in between the deformed mesangial cells (M) and expanded mesangium. [a, X5000 & b, X15000].

Sections of the PCT of the diabetic group exhibited extensive destruction of the apical microvilli with loss of regular basal enfolding. The cytoplasm seemed highly vacuolated with areas of rarified cytoplasm contained scattered heterogenous lysosomes. It contained disorganized mitochondria with abnormal shape and

partially destroyed cristae or even loss of cristae. Nuclei appeared small shrunken pyknotic irregular in shape and condensed heterochromatic with the abnormal distribution of peripheral chromatin. Peritubular collagen fibers cut in different directions were clustered in the areas between the tubules (Fig.11).

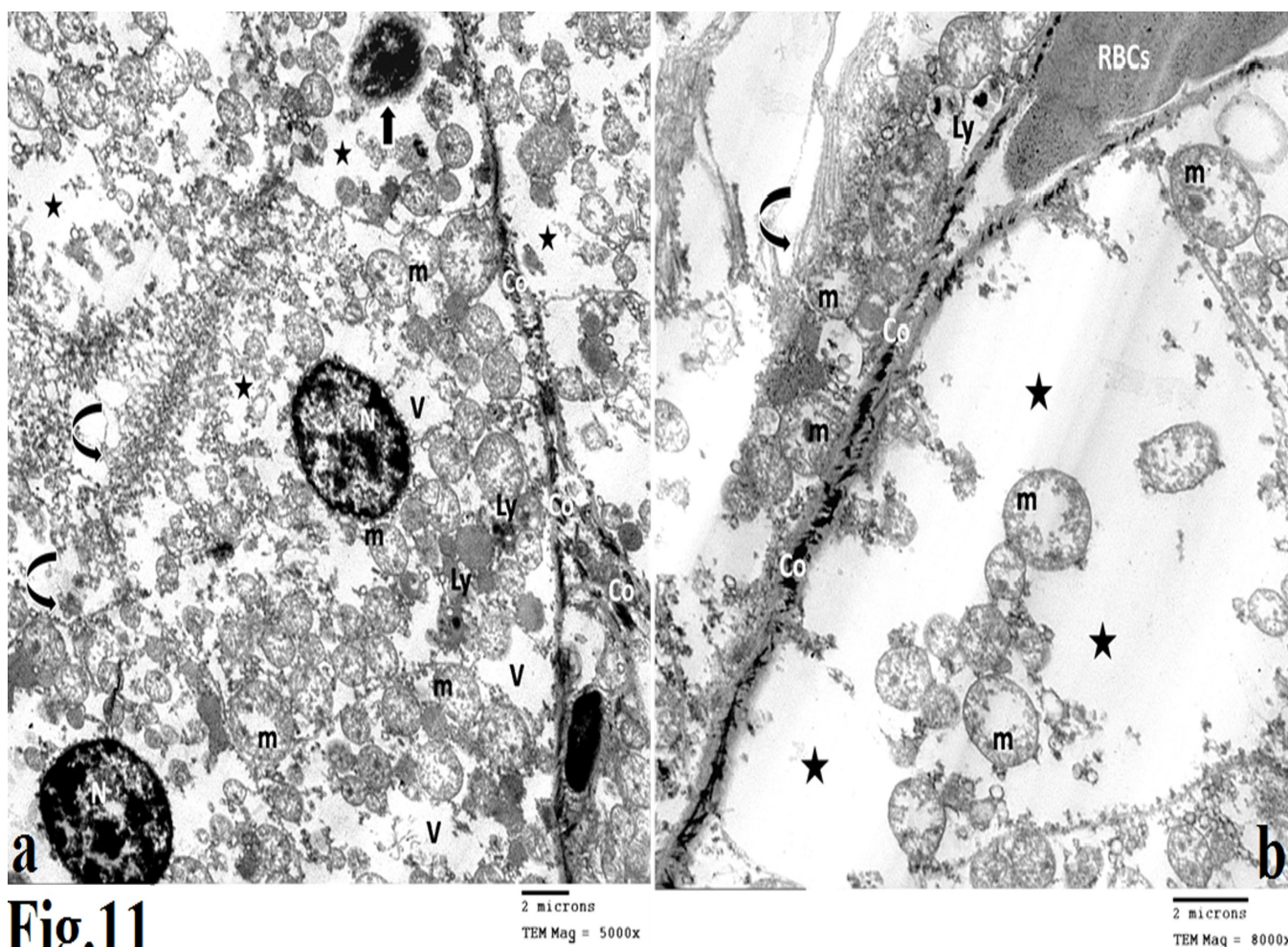


**Fig.11**

**Fig. 11:** TEM of the lining cell of the PCT in the renal cortex of a diabetic rat showing: (a-b) destruction of the apical microvilli (curved arrows) with an absence of regular basal infolding. The nuclei (N) appear distorted, small shrunken pyknotic with condensed heterochromatin and loss of the nuclear envelope (arrow). The cytoplasm seems vacuolated with areas of rarified cytoplasm (stars), large swollen disorganized mitochondria with partially disrupted cristae (m), numerous heterogenous lysosomes (Ly) are also noticed. Between the basement membranes of the tubules there are collagen fibers (Co) cut in different directions and red blood corpuscles (RBCs). [a, X5000 & b, X8000].

The DCTs were severely affected, had disoriented basal infoldings in most cells, dark degenerated mitochondria among abnormal basal folding and disrupted apical border of cells with extrusion of cytoplasm forming ghost body

toward the tubular lumen. Small dark nuclei with irregular chromatin distribution, chromatin clumps and degenerated areas of the cytoplasm with autophagic multiple giant vacuoles were noticed (Fig.12).

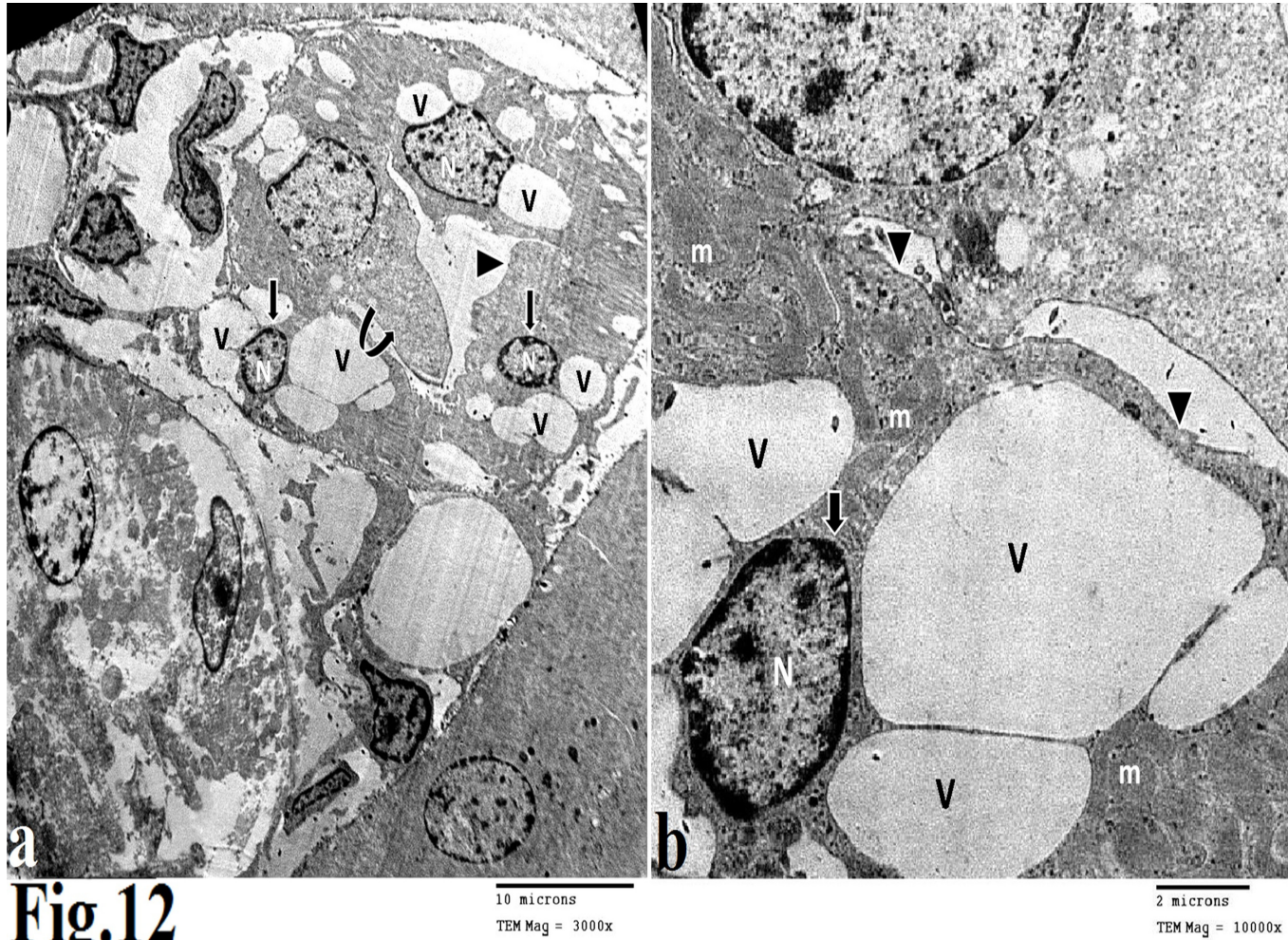


**Fig.12**

**Fig. 12:** TEM of a section in the renal cortex from a diabetic rat showing: (a-b) distorted parts of neighboring cells of the distal and proximal convoluted tubules. Distal convoluted tubular cells appear swollen with the formation of ghost body (curved arrow) and destructed apical microvilli (arrowhead). Small shrunken nuclei (N) with irregular nuclear outline (arrows). The cytoplasm is vacuolated with multiple giant vacuoles (V) and swollen disorganized mitochondria (m) among abnormal basal infolding. [a, X3000 & b, X10000].

Sections of the Diabetic/ MSCs group (GIII) showed a renal structure nearly similar to that of the control group. In the glomerulus, podocyte pedicles were normal in shape except for small effaced areas, broadening, thickened

and fused podocyte feet processes with loss of podocyte pedicles and uneven focal thickening of the glomerular basement membrane, with no evident mesangial matrix expansion (Fig.13).

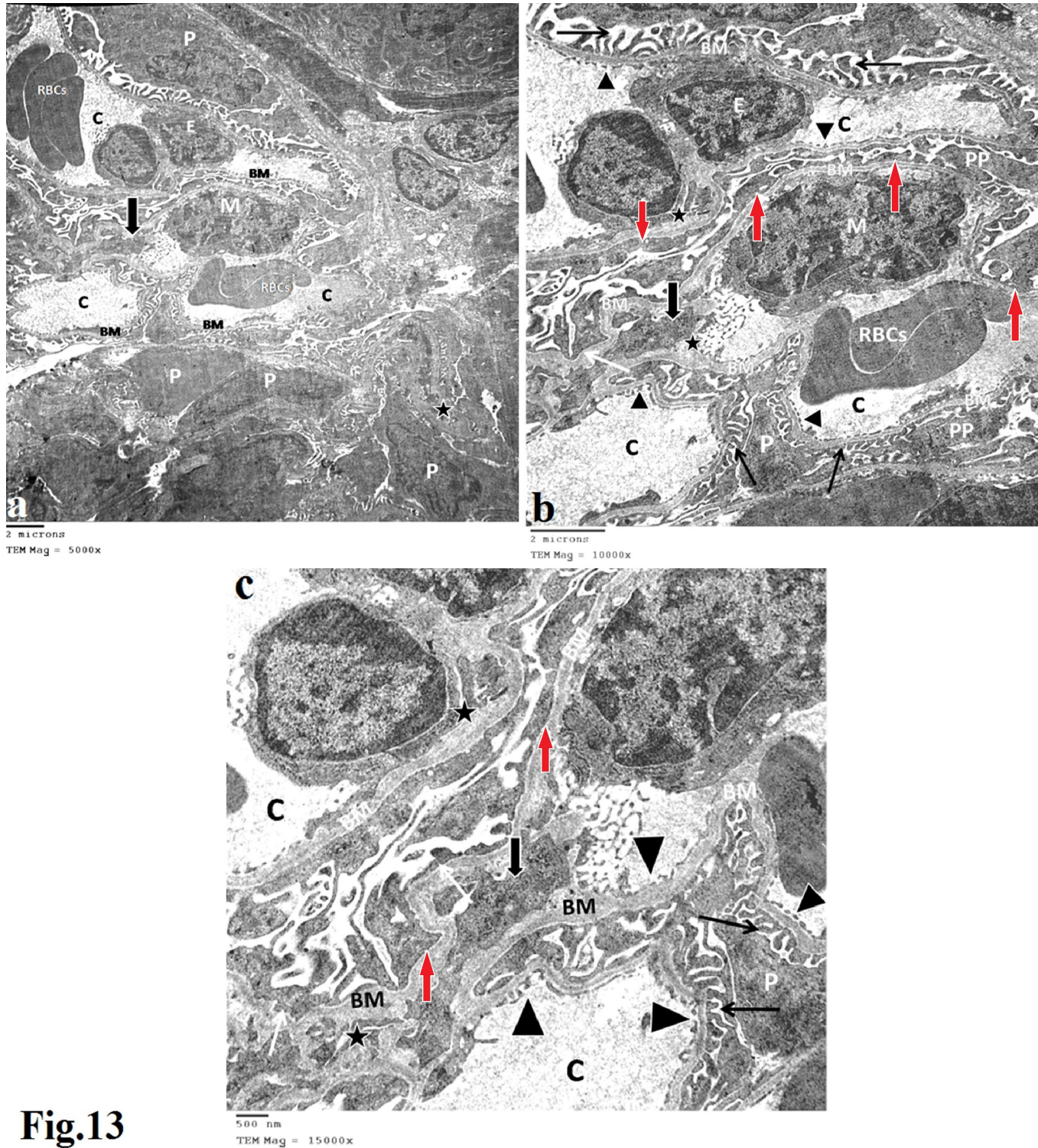


**Fig.13**

**Fig. 13:** TEM of a section in the renal cortex from a diabetic/MSCs treated rat showing: (a-c) a loop of glomerular capillaries (C) contains red blood corpuscles (RBCs), is lined by fenestrated endothelium (arrowhead) and covered by intact podocytes (P). Notice, mesangial cells (M) have a little amorphous mesangial matrix (black arrows). The podocyte (P) has long primary processes (PP) and pedicles (thin arrows) rest on the glomerular capillary surfaces with preservation of the normal glomerular basement membrane (BM) of regular thickness. Notice, a focal thickening (star) of a few parts of the normal glomerular basement membrane. Areas with effaced and fused podocyte feet processes (red arrows) are also seen. [a, X5000; b, X10000 & c, X15000].

Proximal convoluted tubular cells had extensive lateral wall interdigitations, regular basal infoldings enclosed many elongated electron-dense mitochondria surrounded by light spaces, intact regular long microvilli. lysosomes

and some cytoplasmic vacuoles were also observed in their cytoplasm. The basement membrane was irregular and thickened compared to the control group (Fig.14).

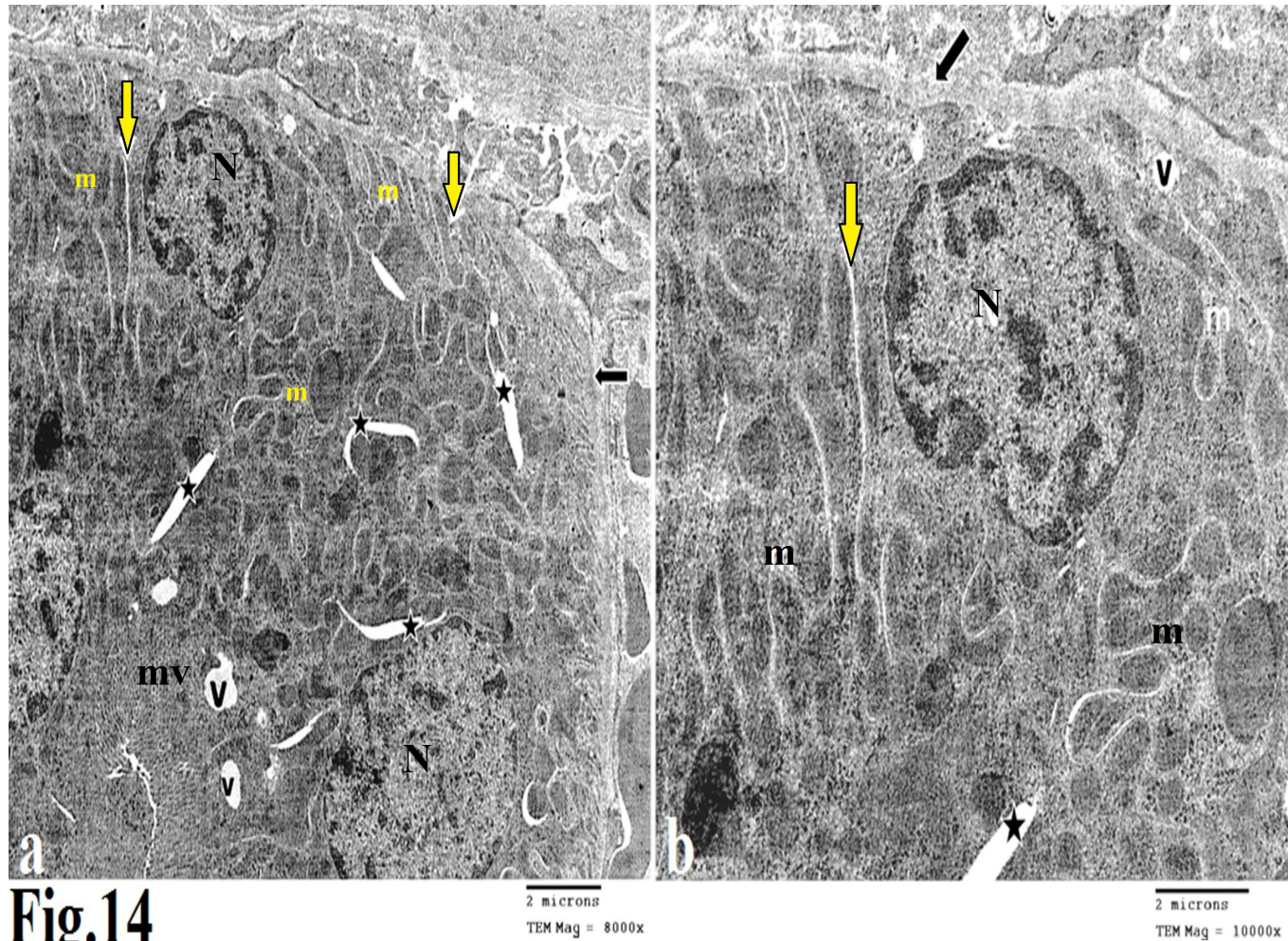


**Fig.14**

**Fig. 14:** TEM of a section in the proximal convoluted tubules from a diabetic/MSCs treated rat showing: (a) preservation of apical microvilli (mv) and normal euchromatic rounded nucleus (N). Basal infolding (yellow arrows) enclosed normal elongated electron-dense mitochondria (m) surrounded by light spaces (stars). The cytoplasm contains some cytoplasmic vacuoles (V) that are more or less similar to those of the control group . Notice, thick regular basement membrane (black arrow) compared to those of the control. [a, X8000 & b, X10000].

Similarly, the DCTs showed a few short apical microvilli, numerous regular basal infoldings, and intact mitochondria. Many small cytoplasmic vacuoles in some

tubular cells were also observed. The nucleus was large with normal peripheral chromatin distribution (Fig.15).

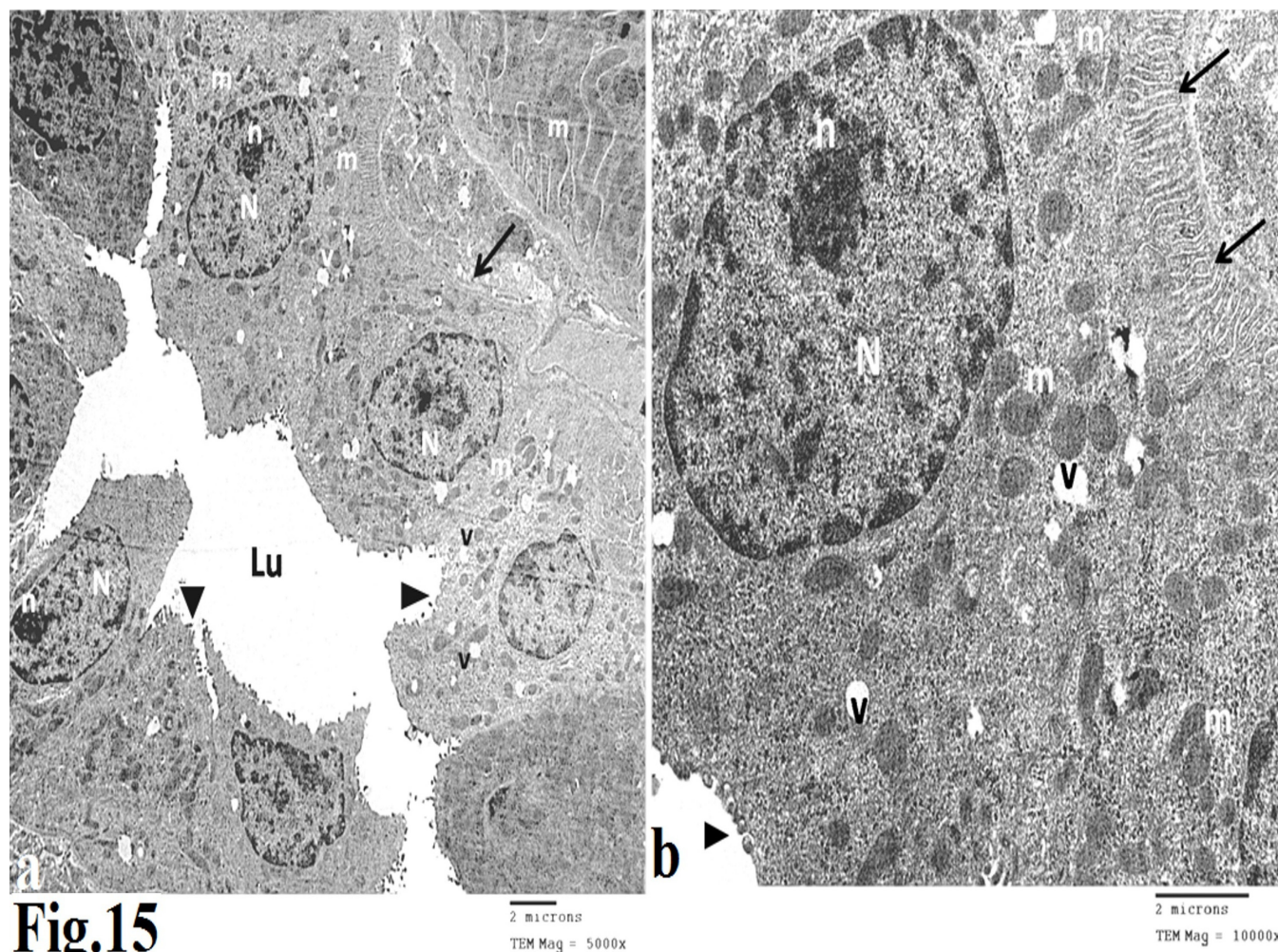


**Fig.15**

**Fig. 15:** TEM of a section in distal convoluted tubule from a diabetic/MSCs treated rat showing: (a) cuboidal cells bulge into the lumen (Lu). (a,b) Irregular and poorly developed blunt apical microvilli (arrowhead) and large spherical, euchromatic nuclei (N) with prominent nucleoli (n). Notice, some small cytoplasmic vacuoles (V) and blunt apical microvilli (arrowhead). (b) multiple normally arranged mitochondria (m) have intact cristae and electron-dense internal matrices. Extensive basal infolding (thin arrows) are more or less similar to those of the control group. [a, X5000 & b, X10000].

**Statistical results:**

The statistical comparison between all control subgroups was nearly similar and revealed no significant difference ( $p > 0.05$ ); therefore, they were referred to as the control group.

**a. Body weight**

The mean values of initial body weight (IBW) of all studied groups were nearly similar with no statistically significant difference. They ranged from  $146.4 \pm 5.9$  to  $147.4 \pm 4.5$

At the end of the experiment, a significant decrease in the mean final body weight (FBW) in the diabetic rats, showed the least recorded mean when compared to the other experimental groups. Upon pre-treatment with MSCs, there was a statistically significant increase in the (FBW) when compared to the diabetic group, but no significant difference was observed compared to the control ( $p > 0.05$ ) [ Table (1) and histogram. (1)].

Table (1): The mean values of initial and final body weight (g) among all the experimental groups.

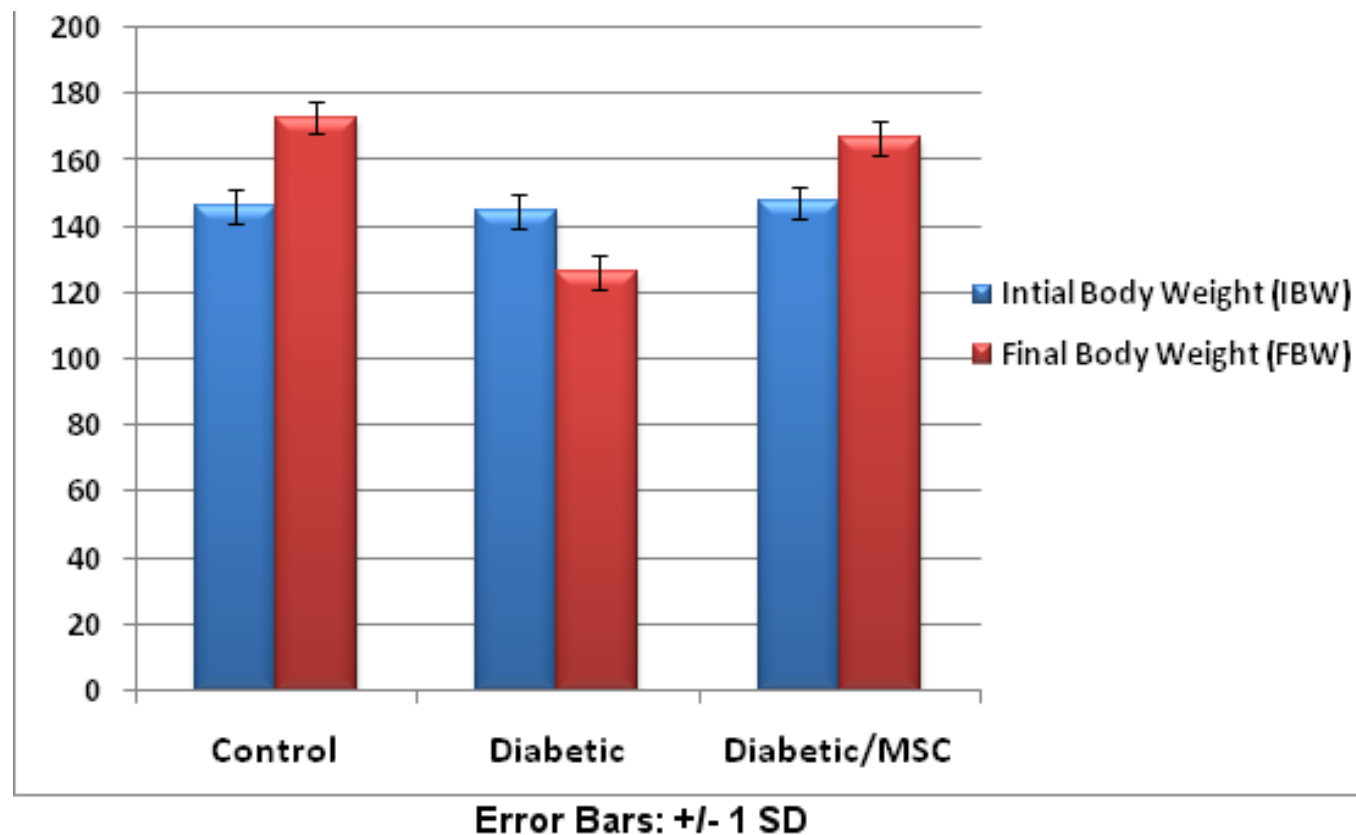
Groups parameters	Group (I) N = 6	Group (II) N = 6	Group (III) N = 6	Test of significance	P
Initial body weight (g)	146.4 ± 5.9	144.9 ± 3.3	147.4 ± 4.5	ANOVA F=0.58	0.6
Final body weight (g)	173 ± 6.5	126.4 ± 5.3	167 ± 4.7	ANOVA F=162	0.000*

Data are presented as means ± standard deviation (SD)

N = Number of animals

\* =  $P \leq 0.05$  = Significant

$P > 0.05$  = Non significant



**Histogram (1): The mean values of initial and final body weight (g) among all the experimental groups.**

**b. Biochemical results:**

**Effect on blood glucose, serum BUN, Creatinine and uric acid**

On the 3<sup>rd</sup> day following STZ injection, the fasting blood glucose levels were within normal in control (G1) (102.5±12.1). However, the highest mean of blood glucose was recorded in Diabetic groups (GII & GIII) 256.9±12.6 & 244.3±7.3 respectively.

At the end of the experiment, diabetic only group (II) showed the highest mean value of blood glucose when compared to the other experimental groups. But, the diabetic / MSCs treated group (III) revealed significant decrease in the mean blood glucose level after eight weeks of MSCs injection when compared with diabetic rats and a non-significant increase when compared with the control group (I) ( $p > 0.05$ ) [Table (2) and Histogram (2)].

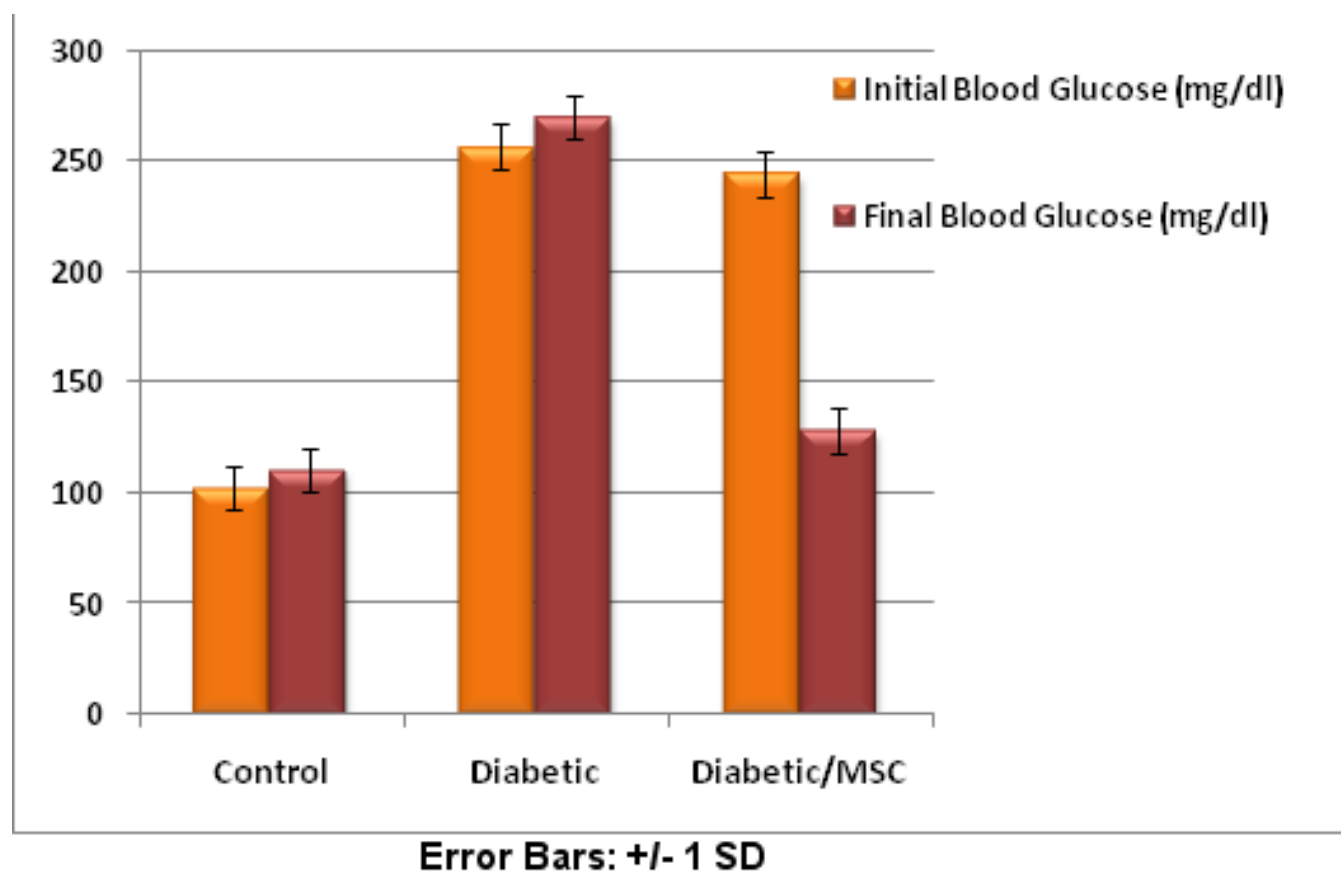
Table (2): The mean values of initial and final blood glucose levels (mg/dl) among the experimental groups.

parameters	Groups			Test of significance	P
	Group (I) N = 6	Group (II) N = 6	Group (III) N = 6		
Initial glucose level (mg / dl)	102.5 ± 12.1	256.9 ± 12.6	244.3 ± 7.3	ANOVA F=20	0.000*
Final glucose level (mg / dl)	110.7 ± 7.9	270.5 ± 16.5	128.3 ± 7.3	ANOVA F=344	0.000*

Data are presented as means ± SD

N = Number of animals

\* =  $P \leq 0.05$  = Significant



**Histogram (2): The mean values of initial and final fasting blood glucose levels (mg/dl) among the experimental groups.**

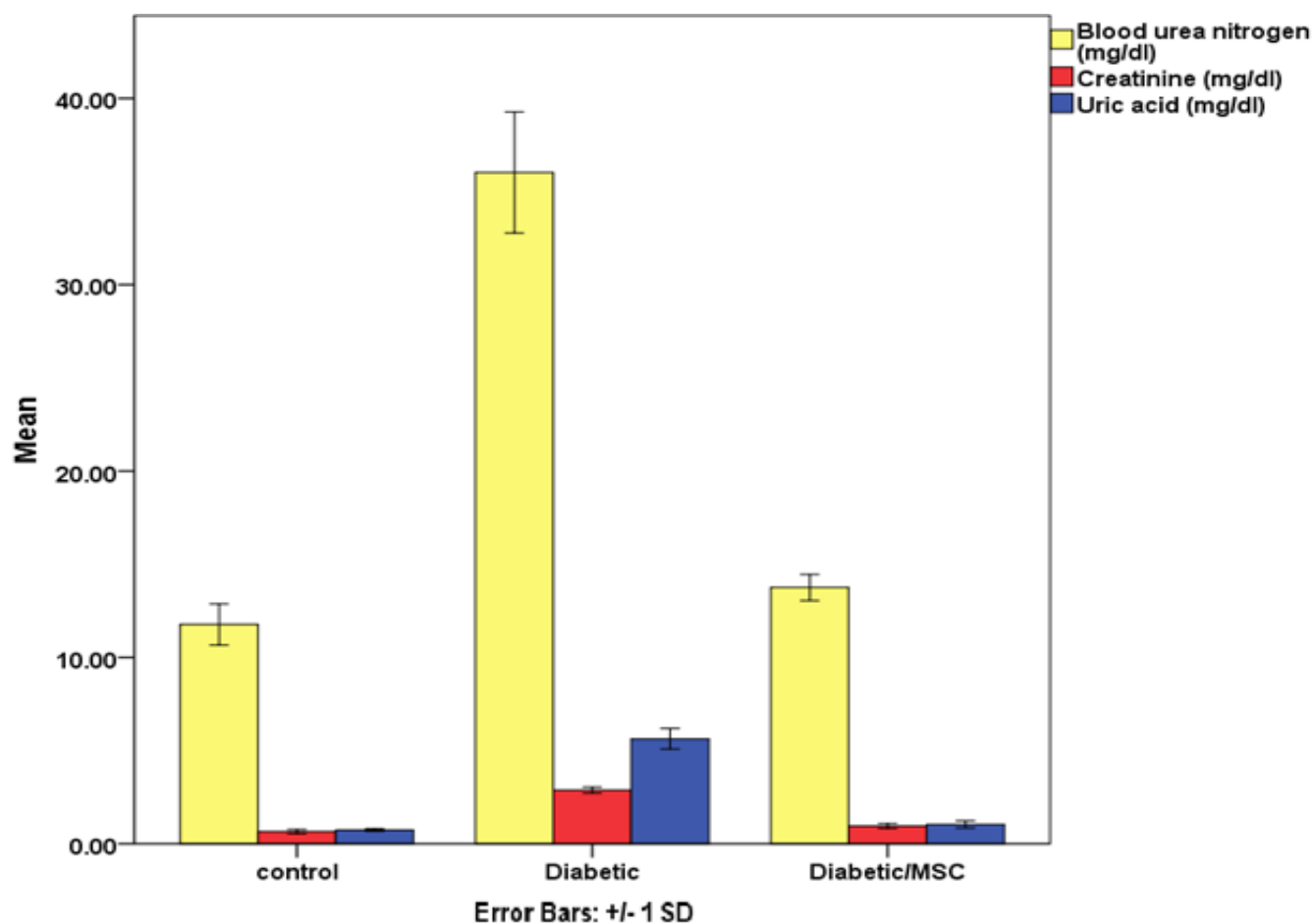
Interestingly, the statistical study concerning serum levels of the BUN, creatinine and uric acid among rats of all groups revealed that the highest mean values were recorded among the diabetic group (II). Inversely, these

parameters were significantly improved if compared with diabetic rats (III) and a non-significant increase if compared with the control rats (I). All these data were represented in Table (3) and Histogram (3).

Table (3): The mean values of serum levels of blood urea nitrogen (BUN), creatinine (Cr) & uric acid (mg/dl) among all the experimental groups.

Groups parameters	Group (I) N = 6	Group (II) N = 6	Group (III) N = 6	Test of significance	P
Blood urea nitrogen (BUN) (mg / dl)	11.8 ± 1.1	36.02 ± 3.2	13.7 ± 0.7	ANOVA F=355	0.000*
Creatinine (Cr) (mg / dl)	0.65 ± 0.1	2.9 ± 0.2	0.95 ± 0.1	ANOVA F=598	0.000*
Uric acid (mg / dl)	0.74 ± 0.2	5.63 ± 0.6	1.04 ± 0.2	ANOVA F=518	0.000*

Data are presented as means ± SD  
 N = Number of animals  
 \* = P ≤ 0.05 = Significant



**Histogram (3): The mean values of serum levels of blood urea nitrogen (BUN), creatinine (Cr) and uric acid (mg/dl) among all the experimental groups.**

**c. Histomorphometric results:**

**1. Area percent of collagen:**

The Using Masson's trichrome stained sections, there was a significant increase in the mean area percentage of collagen fibers in the diabetic rats (GII) versus the control group. Inversely, eight weeks after MSCs injection the

area percentage of collagen fibers significantly decreased in (GIII) when compared with diabetic rats (II) and non-significant increase when compared with the control group [Table (4) and histogram (4)].

## 2. PAS optical density

The optical density of PAS stained sections of the diabetic only group (II) showed the highest mean when compared to the other experimental groups. Inversely, the optical density of diabetic/MSCs treated group (III), showed a significant decrease when compared with diabetic rats and non-significant increase when compared with the control group [Table (4) and histogram (4)].

## 3. The thickness of the glomerular basement membrane (GBM)

The mean values of the GBM of diabetic rats (II) were significantly increased and recorded the highest mean value when compared to control rats (I). Inversely, the mean values of GBM, in the MSCs treated rats (III) revealed a significant decrease when compared with diabetic rats (II) and non-significant difference when compared with the control rats (I) [Table (4) and histogram (4)].

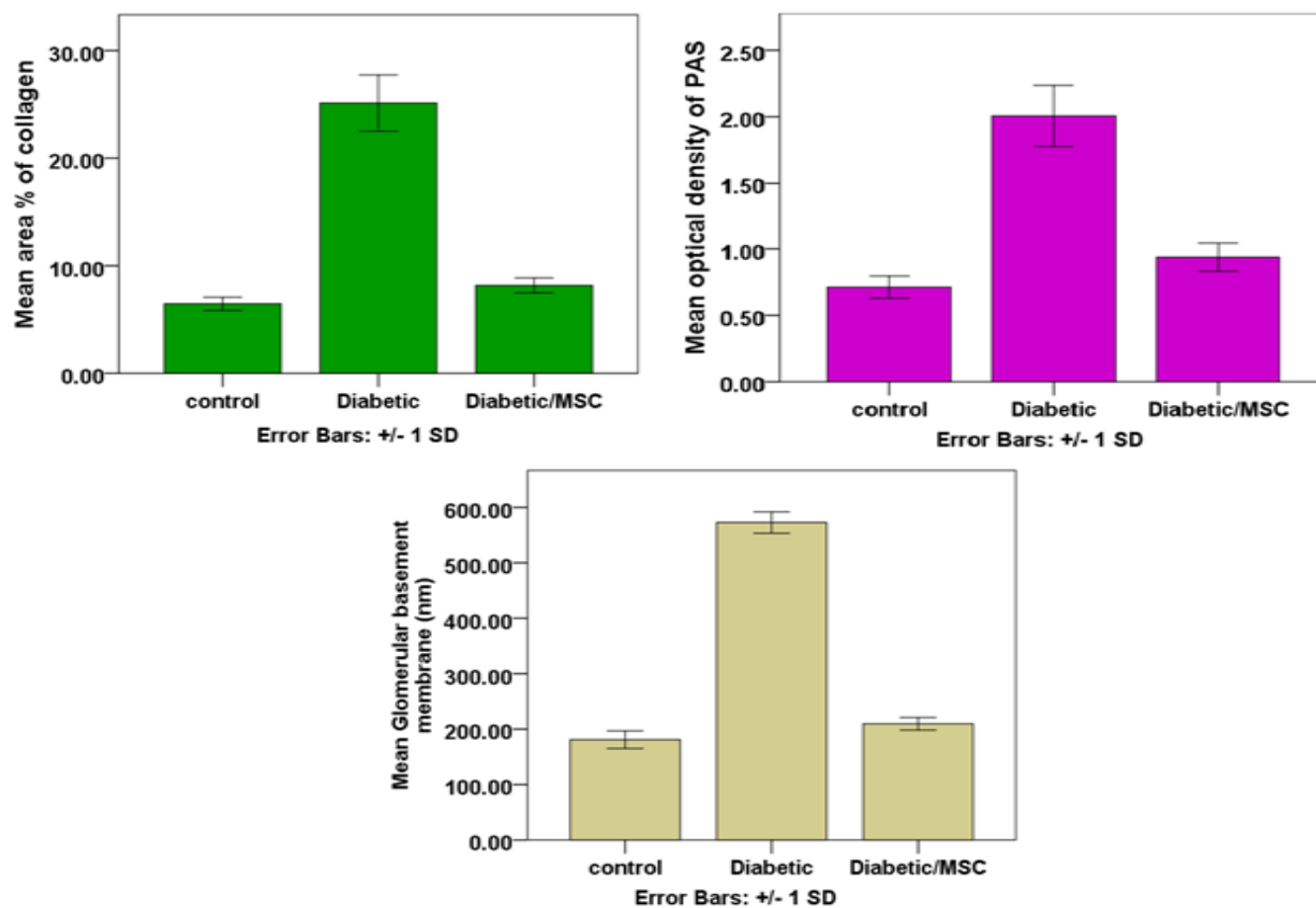
Table (4): The mean values of area % of collagen, PAS optical density and glomerular basement membrane thickness (nm) (mean±SD) among all the experimental groups.

Parameters	Group (I) N = 6	Group (II) N = 6	Group (III) N = 6	Test of significance	P
Area % of collagen	6.5 ± 0.6	25.1 ± 2.6	8.2 ± 0.7	ANOVA F=332	0.000*
PAS optical density	0.71 ± 0.1	1.98 ± 0.2	0.94 ± 0.1	ANOVA F=162	0.000*
Glomerular basement membrane (GBM) thickness (nm)	180.8 ± 15.8	572.7 ± 19.2	209.5 ± 11.3	ANOVA F=1535	0.000*

Data are presented as means ± SD

N = Number of animals

\* =  $P \leq 0.05$  = Significant



**Histogram (4):** The mean values of area % of collagen, PAS optical density and glomerular basement membrane thickness (nm) (mean±SD) among all the experimental groups.

## DISCUSSION

---

Diabetes mellitus, an endocrine and metabolic disorder characterized by chronic hyperglycemia produces multiple biochemical impairments and oxidative stress<sup>[24]</sup>. Disturbed growth factor signaling adversely affects tissue function, changes in the amount and composition of the extracellular matrix (ECM) that influence the development of diabetic complications<sup>[25]</sup>.

Diabetic nephropathy (DN) is one of the most important microvascular complications of diabetes mellitus. It is the most common cause of end-stage renal disease in the world and could account for disability and high mortality rate in patients with type 1 or type 2 diabetes<sup>[26]</sup>. Recent studies have indicated that reactive oxygen species (ROS) plays a key, intermediate role in the development of diabetic nephropathy<sup>[4]</sup>.

Mesenchymal stem cells (MSCs) hold great promise for tissue engineering, cell regeneration and renal repair as well as treating pathophysiology of DN because nephrons are of mesenchymal origin and because stromal cells are of crucial importance for signaling, leading to differentiation of both nephrons and collecting ducts<sup>[27]</sup>. Bone marrow-derived mesenchymal stem cells (BMD-MSCs) has the potential to be more effective than traditional therapies for tissue repair, owing to their capacities to differentiate into replacement cells in damaged tissues, modulate their local environment, secrete various factors and activate endogenous progenitor cells<sup>[28]</sup>.

So, this study aimed to assess the probable renotherapeutic role of bone marrow-derived mesenchymal stem cells (BMSCs) against streptozotocin (STZ) induced nephropathy in adult female albino rats.

Streptozotocin (STZ) was presently used in the induction of diabetes in rats, as; STZ selectively destroys the pancreatic  $\beta$ -cells which inhibits synthesis and release of insulin leading to the onset of diabetes mellitus<sup>[29]</sup>. Experimental evidence has demonstrated that STZ also inhibits free radical scavenger-enzymes apart from the generation of reactive oxygen species (ROS) via induction of oxidative stress<sup>[4]</sup>.

The present study indicated that three days after STZ administration, diabetes was induced as confirmed by elevated blood sugar levels of the rats to  $\geq 200$  mg/dl<sup>[30]</sup>. Eight weeks later, DN was confirmed by serological, histological and ultra-structural measures.

The body-weight loss was a well-documented observation in the diabetic group which may be due to increased catabolism of proteins as a consequence of insulin deficiency which results in the degeneration of structural proteins and muscle wasting<sup>[31]</sup>.

Serum BUN, creatinine and uric acid levels were significantly increased in diabetic rats when compared to those of the controls, indicating renal impairment. This is in agreement with previous studies of Adela *et al.*<sup>[32]</sup> that confirmed the development of DN by increased creatinine and urea, starting 4 weeks after STZ induction of DM in rats and attributed this disturbance to a reduction in glomerular filtration rate, which was correlated with increased creatinine and urea in plasma. Ganugula *et al.*<sup>[33]</sup> explained this disturbance by increased generation of reactive oxygen species (ROS) with high activation of inflammatory signaling cascades, that cause alteration of intraglomerular blood flow and disturbance of the glomerular filtration rate (GFR) as well as alterations of endothelial permeability that linked to cytotoxicity in a variety of cells and ended finally in renal damage observed in DN.

The renal histological findings in the current study went parallel with the serological results as they revealed marked kidney injury. The most prominent signs of kidney deterioration in H & E stained sections of the diabetic rats were in the form of lobulated glomeruli with congested glomerular capillaries, mesangial hypercellularity, severe tubular degeneration, cytoplasmic vacuolation, necrosis, desquamation and sloughing of tubular epithelial cells, with small darkly stained condensed pyknotic nuclei and deterioration of the brush borders of the PCTs presented luminal casts, inflammatory cells infiltration and extravasation of red blood cells.

The possible mechanisms for these structural changes indicated a primary and a secondary effect of the diabetic state on the rat kidney. The primary effect could be explained by the formation of advanced glycation end-products (AGEs) and glucose auto-oxidation following the hyperglycemia that ends in defective cellular glutathione antioxidant system which in turn may induce lipid peroxidation (LPO), cellular necrosis and apoptosis of the renal tissue<sup>[34]</sup>. The secondary effect could be attributed to proinflammatory cytokines, such as interleukin-1 $\beta$  (IL-1 $\beta$ ), IL-6 and tumor necrosis factor-alpha (TNF- $\alpha$ ) with high expression of inducible nitric oxide synthase (iNOS) resulting in oxidative stress, that linked to the tissue parenchymal damage and renal cytotoxicity<sup>[32]</sup>.

Shubin *et al.*<sup>[35]</sup> attributed the cytoplasmic vacuolation, pyknotic nuclei and sloughing of tubular epithelial cells to the free radicals that facilitate the release of lysosomal enzymes and subsequent oxidation of the protein architecture of the cells causing their fragmentation and segregation in vacuoles as a cellular defense mechanism, thus preventing the interference with cellular metabolism.

Desquamation of epithelial tubular cells was explained by the rapid loss of brush border and the disturbance of cytoskeletal integrity with mislocalization of cell adhesion molecules such as the Na<sup>+</sup>/K<sup>+</sup>-ATPase,  $\beta$ - integrins

and adhesion receptors involved in cell-cell adhesion (i.e., vascular endothelial-cadherin catenin complexes). These biologic activities are cytotoxic to renal cells that may induce epithelial sloughing, apoptosis, necrotic cell death and contribute to the progressive renal tubular damage<sup>[35, 36]</sup>.

The intraluminal acidophilic hyaline casts noticed in this study was attributed by El-Achkar *et al.*<sup>[37]</sup> to the combination of the sloughed tubular cells with polymerization of Tamm- Horsfall protein present in the lumen of the tubules and fibronectin as a result of increasing luminal sodium concentration due to impairment of its reabsorption by the damaged tubular cells forms a gel-like material contributing in cast formation.

The inflammatory cells infiltration detected in the current study might be due to the ability of STZ to induce inflammatory reactions by increasing neutrophil-endothelial cell interactions with subsequent release of proinflammatory, profibrotic, and antiangiogenic factors from the activated neutrophils, macrophages and lymphocytes including TNF- $\alpha$ , IL-1, IL-6, ROS, plasminogen activator inhibitor-1 (PAI-1), matrix metalloproteinases, transforming growth factor-beta (TGF  $\beta$ ), platelet-derived growth factor (PDGF), angiotensin II, acute phase proteins and endothelin mediating kidney inflammation in experimental and human diabetes<sup>[38]</sup>.

In the present study, a significant increase in the density and distribution of collagen fibers within the renal interstitium diabetes-induced nephropathy group in Masson's trichrome-stained sections was most probably due to reactive oxygen species overproduction, apoptosis dysregulation and increase proinflammatory cytokines expressions which increased the activity of mesangial cells, matrix remodeling and locally produced a fibrogenic growth factor TGF- $\beta$  and nuclear transcription factor-Kappa-B (NF- $\kappa$ B)<sup>[39]</sup> which might induce transformation of tubular epithelial cells to myofibroblast, through epithelial-mesenchymal transition (EMT) that is the major source of extracellular matrix secretion ending up with progressive renal interstitial fibrosis<sup>[40]</sup>.

A significant increase in the optical density of PAS-positive reaction at the glomerular, capsular and tubular basement membranes and mesangial matrix with apparent thickening of basement membranes that was observed in the diabetic group could be attributed to the increased deposition of intraglomerular mesangial matrix glycoproteins<sup>[41]</sup>, up-regulation of integrins, laminin and fibronectin secondary to increased collagen fiber formation with subsequent increase in basement membrane thickness<sup>[42, 43]</sup>.

Furthermore, loss of the apical brush border and faint PAS-positive materials that were observed in the PCTs could be explained according to Forbes and Cooper<sup>[44]</sup> to the leakages of enzymes associated with the apical brush borders such as gamma-glutamyltransferase (GGT) and alkaline phosphatase (AP) enzymes as a result of the disturbance of cytoskeletal integrity and epithelial detachment.

A classic morphological tubular change in the form of intracytoplasmic PAS-positive granules with the appearance of Armanni-Ebstein cells has been reported in the proximal tubular epithelial cells in the diabetic rats. This phenomenon of abnormal glycogen deposits was resulting from alteration in glucose metabolism concomitant with excessive excretion of glycogen through the glomeruli that are reabsorbed and accumulated within the tubular epithelial cells. The accumulated cytoplasmic glycogen particles result in cytoplasmic vacuolization during the H&E staining procedure and could be detected by PAS-positive reaction<sup>[43]</sup>. It is frequently seen in diabetic patients with heavy glycosuria<sup>[45]</sup>.

Electron microscopic examination of the renal cortex of the diabetic group confirmed all findings depicted previously with diffuse thickening of the pericapsular and glomerular basement membranes with indistinct layers, accumulation of the mesangial matrix, areas of subepithelial electron-dense hyalinosis with increased intraglomerular mesangial matrix expansion, deteriorated podocytes, broadening, effacement and fusion of their foot process, loss of fenestration of endothelial cells of the capillaries as well as deformed mesangial cells. The EM examination of renal tubules showed damage of proximal and distal convoluted tubules in the form of vacuolization of the renal tubular cells and disturbed microvilli, small apoptotic irregular nuclei with chromatin condensation, loss of the nuclear envelope and disorganized mitochondria with disrupted cristae. Moreover, electron-dense mitochondria in between disorganized basal infoldings were also observed in the distal convoluted tubules.

Thickening of the GBM was attributed to oxidative stress, production of inflammatory cytokines and growth factors resulting in enhanced production of constitutional extracellular matrix components of the GBM from podocytes or glomerular endothelial cells, excessive collagen type IV deposition and impairment of excess extracellular matrix degradation in DN<sup>[46]</sup>.

Moreover, the modification of GBM molecular structure by non-enzymatic glycation produces AGEs with architecture resistant against tissue metalloproteinases along with pericapsular fibrosis, is another theory described recently by Marshall<sup>[42]</sup>.

Studies by Arif and Nihalani<sup>[47]</sup> have implicated high glucose-induced oxidative stress, free oxygen radicals, TGF- $\beta$  and proapoptotic mitogen-activated protein kinases (MAPK) p38 signaling during diabetic nephropathy trigger apoptosis of the mesangial cells and podocytes coincided with the progression of glomerular dysfunction.

Peired *et al.*<sup>[48]</sup> proposed that the underlying mechanisms leading to foot process effacement and degeneration include; changes in slit diaphragm-associated proteins, actin cytoskeleton abnormalities, alterations in the negative apical membrane domain of podocytes, and interference with podocyte-GBM interaction due to reduced expression of the  $\alpha 3\beta 1$  integrin, the predominant integrin tethering the podocyte to the GBM.

Hyalinosis and non-specific mesangial fibrils (diabetic fibrosis) are probably secondary to chronic mesangial injury<sup>[49]</sup>.

Eventually, persistent podocyte injury, hyalinosis with mesangial expansion together with glomerular basement membrane thickening is a typical characteristic of renal dysfunction during development and/or progression of diabetic nephropathy with consecutive glomerulosclerosis and tubulointerstitial fibrosis which eventually progress to end-stage renal failure requiring dialysis worldwide<sup>[47, 50]</sup>.

Notable degenerative changes of the tubular epithelial cell and in the mitochondria in the present study were explained by STZ-induced apoptosis, where oxidative stress following STZ activated P53 in renal tubular cells and upregulated the proapoptotic genes that trigger changing the mitochondrial inner membrane composition, translocation of intra-mitochondrial protein (apoptosis-inducing factor), opening the mitochondrial permeability transition pore with subsequent release of apoptogenic factors, damaging mitochondrial DNA directly with ATP depletion ending with structural alterations of the matrix, mitochondrial swelling and cell death through the autophagic and apoptotic pathway<sup>[51, 52]</sup>. Nuclear pyknosis was likely a representation of cells undergoing apoptosis and atrophic degeneration secondary to increased reactive oxygen species (ROS) that could alter repair enzymes and DNA polymerases which ran parallel to the DNA damage-inducing mutations<sup>[52]</sup>.

The present MSCs injection 72 hours after STZ injection in diabetic group revealed marked improvement in the serological, histological and ultrastructural parameters of the kidney, restoration of the architecture of renal corpuscles, PCTs and DCTs as compared to the DN group. However, their levels couldn't reach normal levels. These findings are in accordance with studies of Abdel Aziz *et al.*<sup>[12]</sup> who stated that the administration of MSCs tended to significantly reduce serum urea and creatinine and improve kidney function as well as the preservation of normal renal histology.

The MSC treated group exhibited nearly similar ultrastructure to that of the control group except for small areas with effaced and fused podocyte feet processes that were confirmed by a significant decrease in the GBM thickness when compared with diabetic rats and nonsignificant difference when compared with the control rats.

The precise mechanisms of action of MSCs as attractive candidates for renal repair in preclinical models of DN have not been fully elaborated. Wu *et al.*<sup>[53]</sup> indicated that the reno-protective effect of MSCs may be due to indirect effect i.e. hyperglycemia correction and improved microalbuminuria which subsequently improves kidney function<sup>[53]</sup>.

Zhu *et al.*<sup>[54]</sup> added that MSCs may ameliorate the kidney directly i.e. due to protection/regeneration and proliferation of renal tissue.

According to Li *et al.*<sup>[55]</sup>, cellular damage may stimulate the recruitment of multipotent adult stem cells to migrate, insinuate themselves, engraft in damaged kidneys and receive signals that direct proliferation and subsequent trans-differentiation into renal cells to repopulate renal tubules resulting inefficient treatment of DN. This was confirmed by Prussian blue light microscopic results. Similar findings have been reported by Morigi *et al.*<sup>[56]</sup> who detected red fluorescence-labeled human bone marrow MSCs with PKH 26 dye clearly in renal tissues into mice with induced acute renal failure.

Also, Ni *et al.*<sup>[57]</sup> declared that bone-marrow derived cells may home to injured glomerular endothelium, differentiate into endothelial cells, and participate in the angiogenesis and regeneration of the highly specialized glomerular microvasculature. Wu *et al.*<sup>[53]</sup> added that the MSCs trans-differentiation might be only a small part of the mechanism by which, MSCs could exert their therapeutic effect.

Li and Wingert<sup>[58]</sup> stated that regeneration of renal tubular and glomerular cell populations using bone marrow-derived stem cells (BMDSCs) is merely cytokine-induced renal improvement and the majority of reparative cells were derived from intrinsic kidney cells resulting in the observed functional repair.

Cell fusion between transplanted BMSCs and recipient tissue has been claimed as an alternative mechanism to trans-differentiation, which can occur in vivo and produce functional cells in the injured tissues<sup>[55]</sup>. Meanwhile, direct contact of MSCs with the cellular microenvironment could stimulate asymmetric divisions of stem cells in renal niches and their differentiation into tubular cells.

An expanding number of data attributed the therapeutic effects of MSCs to paracrine mechanisms through the secretion of various trophic factors such as vascular endothelial growth factor (VEGF), basic fibroblast growth factor (b-FGF), monocyte-chemoattractant protein-1 and insulin growth factor-1 (IGF-1)<sup>[12]</sup> and the potency of MSCs to modulate local environment, activate endogenous progenitor cells and immunomodulation<sup>[59]</sup>.

Reduction in the interstitial inflammation in diabetic/ MSCs treated group was attributed to the anti-inflammatory effect of MSCs on T cells or natural killer (NK) cells, suppression of B lymphocyte proliferation as well as antibody production, possibly stimulating regulatory T cells, downregulation of proinflammatory cytokines such as TNF- $\alpha$ , interferon- $\gamma$  (IFN- $\gamma$ ) and fibrogenic growth factors<sup>[60]</sup>. Furthermore, MSCs could up-regulate organ-protective Interleukin-10 (IL-10) which is an antifibrotic agent because of its well-known role as an anti-inflammatory mediator which reduced the deposition of extracellular matrix in the renal interstitium and markedly decreased tubulointerstitial fibrosis<sup>[61]</sup>.

## CONCLUSION

The injection of BMSCs was considered as one of the new effective strategies for STZ-induced nephropathy in adult female albino rats. Although the mechanisms responsible for their protective and regenerative effects are incompletely understood, MSC could decrease the progression of DN in diabetic rats most probably through their paracrine action, anti-inflammatory, immunoregulatory properties of MSCs and decreased mitochondrial apoptosis pathway with the increased proliferative ability of the tubular cells which was confirmed by decreased blood glucose levels, improved renal function, histopathology and ultrastructure of renal cortical tissue.

## CONFLICT OF INTEREST

There are no conflicts of interest.

## FUNDING

This study was not funded by any source.

## REFERENCES

1. Sulaiman MK. Diabetic nephropathy: recent advances in pathophysiology and challenges in dietary management. *Diabetology and Metabolic Syndrome* 2019; 11(7):1-5.
2. Lakshmipathi J, Alvarez-Perez J C, Rosselot C, Casinelli GP, Stamateris RE, Rausell-Palamos F, O'Donnell CP, Vasavada RC, Scott DK, Alonso LC and Garcia-Ocaña A. PKC $\zeta$  is essential for pancreatic  $\beta$ -cell replication during insulin resistance by regulating mTOR and cyclin-D2. *Diabetes* 2016; 65(5): 1283–1296.
3. Kawanami D, Matoba K and Utsunomiya K: Dyslipidemia in diabetic nephropathy . *Renal Replacement Therapy* 2016; 2(16):7-24.
4. Jha JC, Banal C, Chow BS, Cooper ME and Jandeleit-Dahm K: Diabetes and Kidney Disease: Role of Oxidative Stress. *Antioxidants and Redox Signaling* 2016; 25(12): 657 -684.
5. Kato M and Natarajan R. Diabetic nephropathy - emerging epigenetic mechanisms. *Nat Rev Nephrol.* 2014; 10(9):517–530.
6. Lozano-Maneiro L and Puente-Garcia A. Renin-Angiotensin-Aldosterone Blockade in Diabetic Nephropathy. Present Evidences. *J Clin Med.* 2015; 4(11):1908-1937.
7. Volarevic V, Al-Qahtani A, Arsenijevic N, Pajovic S and Lukic ML. Interleukin-1 receptor antagonist (IL-1Ra) and IL-1Ra producing mesenchymal stem cells as modulators of diabetogenesis. *Autoimmunity* 2010, 43(4):255–263.
8. Lee JS, Hong JM, Moon GJ, Ahn YH, Bang OY: A long-term follow-up study of intravenous autologous mesenchymal stem cell transplantation in patients with ischemic stroke. *Stem Cells* 2010, 28(6):1099–1106.
9. Richardson SM, Kalamegam G, Pushparaj PN, Matta C, Memic A, Khademhosseini A, Mobasheri R, Poletti FL, Hoyland JA and Mobasheri A. Mesenchymal stem cells in regenerative medicine: focus on articular cartilage and intervertebral disc regeneration. *Methods.* 2016; 99(2016):69–80.
10. Abu Abeeleh M, Bani Ismail Z and Alzaben KR. Induction of Diabetes Mellitus in Rats Using Intraperitoneal Streptozotocin: A Comparison between 2 Strains of Rats. *European Journal of Scientific Research.* 2010; 32 (3): 398-402.
11. Zhou H, Tian H, Long Y, Zhang XX, Zhong L, Deng L, Chen XH and Li XQ. Mesenchymal stem cells transplantation mildly ameliorates experimental diabetic nephropathy in rats. *Chin Med J* 2009; 122(21):2573–2579.
12. Abdel Aziz MT, Abdel Wassef M, Ahmed HH, Rashed L, Mahfouz S, Aly MI, Hussein RE and Abdelaziz M. The role of bone marrow derived-

- mesenchymal stem cells in attenuation of kidney function in rats with diabetic nephropathy. *Diabetology & Metabolic Syndrome* 2014; 6(34):1-10.
13. Shah HR, Arivarasan A, Kumar P and Ambasta RK. Protective effects of transplanted bone marrow mononuclear cells (BMMNCs) in organ damage caused due to streptozotocin (STZ) induced diabetes. *Research. African Journal of Pharmacy and Pharmacology* 2011; 5 (23): 2605-2612.
  14. El Said HE, Gabr HM and Ammar RI. The effect of human bone marrow mesenchymal stem cells on diabetic heart failure rats. *Life Sci J.* 2013; 10 (1): 3413 -3425.
  15. Ellis R. Perls Prussian Blue Stain Protocol, Pathology Division, Queen Elizabeth Hospital. South Australia. 2007.
  16. Ngen EJ, Wang L, Kato Y, Krishnamachary B, Zhu W, Gandhi N, Smith B, Armour M, Wong J, Gabrielson K and Artemov D. Imaging transplanted stem cells in real time using an MRI dual-contrast method. *Scientific Reports* 2015; 5:ID13628 .1-13.
  17. Merghani BH, Awadin WF, Elseady YY and Abu-Heakal NSA. Protective Role of Wheat Germ Oil against Hyperglycemia and Hyperlipidemia in Streptozotocin Induced Diabetic Rats. *Asian Journal of Animal and Veterinary Advances* 2015 10 (12): 852-864.
  18. Bancroft JD and Layton C. The hematoxylin and eosin, connective mesenchymal tissues with their stains In: Suvarna SK, Layton C and Bancroft JD (eds). *Bancroft's Theory and practice of histological techniques.* (7<sup>th</sup> edition). Churchill Livingstone, Philadelphia. 2013; pp 173-212 and 215-238.
  19. Hayat MA: *Principles and Techniques of Electron Microscopy: Biological Applications.* 4th ed. Cambridge university press, Cambridge, United Kingdom. 2000; pp 85-138.
  20. Izbicki G, Segel MJ, Christensen TG, Conner MW and Breuer R. Time course of bleomycin-induced lung fibrosis. *International journal of experimental pathology* 2002; 83(3):111-119.
  21. AbdelKader DH, Gabri MS, Ibrahim MA and Hassan BN. Histological and Immunohistochemical study on the Changes Induced by Contraceptive pills in the female rabbit's kidney. *The Egyptian Journal of Hospital Medicine* 2012; 46(1): 47 – 63.
  22. Aboulkhair AG, Sabry M and Rabiee A. A possible mechanism of the protective effect of simvastatin on streptozotocin induced diabetic nephropathy in adult male rats (a histological study) *Journal of Medical Histology* 2017; 1 (1): 84-96.
  23. McHugh ML. Multiple comparison analysis testing in ANOVA. *Biochemia Medica* 2011; 21(3):203-209.
  24. Tangvarasittichai S. Oxidative stress, insulin resistance, dyslipidemia and type 2 diabetes mellitus. *World J Diabetes* 2015; 6(3): 456-480.
  25. Marika B, Eva K, Charmaine JS, Christopher RP, Lydia S and Thomas NW. Extracellular Matrix Components in the Pathogenesis of Type 1 Diabetes. *Curr Diab Rep.* 2014; 14(12): 552-557.
  26. Chawla A, Chawla R and Jaggi S. Microvascular and macrovascular complications in diabetes mellitus: Distinct or continuum? *Indian J Endocrinol Metab.* 2016; 20(4):546-551.
  27. Davey GC, Patil SB, O'Loughlin A and O'Brien T. Mesenchymal Stem Cell-Based Treatment for Microvascular and Secondary Complications of Diabetes Mellitus. *Front Endocrinol (Lausanne)* 2014; 5(86):1-16.
  28. Krause M, Rak-Raszewska A, Pietilä I, Quaggin SE and Vainio S. Signaling during Kidney Development. *Cells* 2015; 4(2): 112–132.
  29. Al-Quraishy S, Dkhil MA, Abdel Moneim AE. Anti-hyperglycemic activity of selenium nanoparticles in streptozotocin-induced diabetic rats. *Int J Nanomedicine* 2015; 10: 6741- 6756.
  30. Ahmad U and Ahmad RS. Anti diabetic property of aqueous extract of *Stevia rebaudiana* Bertoni leaves in Streptozotocin-induced diabetes in albino rats. *BMC Complement Altern Med.* 2018; 18(179):1-11.
  31. Rasineni KR, Bellamkonda SR and Singareddy DS. Antihyperglycemic activity of *Catharanthus roseus* leaf powder in streptozotocin-induced diabetic rats. *Pharmacognosy research* 2010; 2(3):195-201.
  32. Adela R, Nethi SK, Bagul PK, Barui AK, Mattapally S, Kuncha M, Patra CR, Reddy NC and Banerjee SK. Hyperglycaemia Enhances Nitric

- Oxide Production in Diabetes: A Study from South Indian Patients .PLoS One 2015; 10(4): 1-17.
33. GanugulaR, AroraM, JaisamutP, Wiwattanapatapee R, Jørgensen HG, Venkatapurwar VP, Zhou B, Hoffmann AR, Basu R, Guo Sh. and Majeti NVK. Nano-curcumin safely prevents streptozotocin-induced inflammation and apoptosis in pancreatic beta cells for effective management of Type 1 diabetes mellitus *Br J Pharmacol.* 2017 ; 174(13): 2074–2084.
  34. Nowotny K, Jung T, Höhn A, Weber D and Grune T. Advanced Glycation End Products and Oxidative Stress in Type 2 Diabetes Mellitus *Biomolecules* 2015; 5(1): 194-222.
  35. Shubin AV, Demidyuk IV, Komissarov AA, Rafieva LM and Kostrov SV. Cytoplasmic vacuolization in cell death and survival Oncotarget. 2016; 7(34): 55863–55889.
  36. Mittal M, Siddiqui MR, Tran K, Reddy SP and Malik AB. Reactive Oxygen Species in Inflammation and Tissue Injury. *Antioxid Redox Signal.* 2014; 20(7): 1126–1167.
  37. El-Achkar TM, McCracken R, Liu Y, Heitmeier MR, Bourgeois S, Ryerse J, and Xue-Ru W. Tamm-Horsfall protein translocates to the basolateral domain of thick ascending limbs, interstitium, and circulation during recovery from acute kidney injury *Am J Physiol Renal Physiol.* 2013; 304(8): F1066–F1075.
  38. Yamamoto Y and Yamamoto H. Controlling the receptor for advanced glycation end products to conquer diabetic vascular complications. *J Diabetes Investig.* 2012; 3(2): 107–114.
  39. Kendall RT and Feghali-Bostwick CA. Fibroblasts in fibrosis: novel roles and mediators *Front Pharmacol.* 2014; 5(123): 1-13.
  40. Nogueira A, Pires MJ and Oliveira PA. Pathophysiological Mechanisms of Renal Fibrosis: A Review of Animal Models and Therapeutic Strategies *In Vivo* 2017; 31(1): 1–22.
  41. Byron A, Randles MJ, Humphries JD, Mironov A, Hamidi H, Harris S, Mathieson PW, Saleem MA, Satchell SC, Zent R, Humphries MJ and Lennon R. Glomerular cell cross-talk influences composition and assembly of extracellular matrix. *J Am Soc Nephrol.* 2014; 25(5): 953–966.
  42. Marshall CB. Rethinking glomerular basement membrane thickening in diabetic nephropathy: adaptive or pathogenic? *Am J Physiol Renal Physiol.* 2016; 311(5): F831–F843.
  43. Vallon V and Komers R. Pathophysiology of the Diabetic Kidney *Compr Physiol.* 2011; 1(3): 1175–1232.
  44. Forbes JM, Cooper ME. Mechanisms of diabetic complications. *Physiol Rev.* 2013; 93(1): 137–188.
  45. Vallon V and Homson SC. Renal Function in Diabetic Disease Models: The Tubular System in the Pathophysiology of the Diabetic Kidney *Annu Rev Physiol.* 2012; 74(1): 1-27.
  46. Pichaiwong W, Hudkins KL, Wietecha T, Nguyen TQ, Tachaudomdach C, Li W, Askari B, Kobayashi T, O'Brien KD, Pippin JW, Shankland SJ, and Alpers CE. Reversibility of structural and functional damage in a model of advanced diabetic nephropathy. *J Am Soc Nephrol.* 2013; 24(7):1088–1102.
  47. Arif E and Nihalani D. Glomerular Filtration Barrier Assembly: An insight. *Postdoc J.* 2013; 1(4): 33–45.
  48. Peired A, Angelotti ML, Ronconi E, Marca GL, Mazzinghi B, Sisti A, Lombardi D, Giocaliere E, Bona MD, Villanelli F, Parente E, Ballerini L, Sagrinati C, Wanner N, Huber TB, Liapis H, Lazzeri E, Lasagni L and Romagnani P. Proteinuria impairs podocyte regeneration by sequestering retinoic Acid. *J Am Soc Nephrol.* 2013; 24(11):1756–1768.
  49. Maezawa Y, Takemoto M and Yokote K. Cell biology of diabetic nephropathy: Roles of endothelial cells, tubulointerstitial cells and podocytes. *Journal of Diabetes Investigation* 2015; 6 (1): 3–15.
  50. Anil Kumar P, Welsh GI, Saleem MA and Menon RK. Molecular and cellular events mediating glomerular podocyte dysfunction and depletion in diabetes mellitus. *Front Endocrinol (Lausanne)* 2014; 5(151):1-10.
  51. Havasi A and Dong Z. Autophagy and tubular cell death in the kidney *Semin Nephrol.* 2016; 36(3): 174–188.

52. Kimura T, Takahashi A, Takabatake Y, Namba T, Yamamoto T, Kaimori J-Y, Matsui I, Kitamura H, Niimura F, Matsusaka T, Soga T, Rakugi H and Isaka Y. Autophagy protects kidney proximal tubule epithelial cells from mitochondrial metabolic stress. *Autophagy* 2013; 9 (11):1876–1886.
53. Wu J, Ji C, Cao F, Lui H, Xia B and Wang L. Bone marrow mesenchymal stem cells inhibit dendritic cells differentiation and maturation by microRNA-23b. *Biosci Rep.* 2017; 37 (2): 1-10.
54. Zhu W, Yuan Y, Liao G, Li L, Liu J, Chen Y, Zhang J, Cheng J and Lu Y. Mesenchymal stem cells ameliorate hyperglycemia-induced endothelial injury through modulation of mitophagy. *Cell Death Dis.* 2018; 9 (837): 1-17.
55. Li Y, Liu J, Liao G, Zhang J, Chen Y, Li L, Liu F, Chen B, Guo G, Wang C, Yang L, Cheng J and Lu Y. Early intervention with mesenchymal stem cells prevents nephropathy in diabetic rats by ameliorating the inflammatory microenvironment. *Int J Mol Med.* 2018; 41(5):2629-2639.
56. Morigi M, Inrona M, Imberti B, Corna D, Abbate M, Rota C, Rottoli D, Benigni A, Perico N, Zoja C, Rambaldi A, Remuzzi A and Remuzzi G. Human bone marrow mesenchymal stem cells accelerate recovery of acute renal injury and prolong survival in mice. *Stem Cells* 2008; 26(8):2075–2082.
57. Ni W, Fang Y, Xie L, Liu X, Shan W, Zeng R, Liu J and Liu X. Adipose derived mesenchymal stem cells transplantation alleviates renal injury in streptozotocin-induced diabetic nephropathy. *J Histochem Cytochem.*2015; 63(11):842–853.
58. Li Y and Wingert RA. Regenerative medicine for the kidney: stem cell prospects & challenges *Clin Transl Med.* 2013; 2(11):1-16.
59. Park JH, Jang HR, Kim DH, Kwon GY, Lee JE, Huh W, Choi SJ, Oh W, Oh HY and Kim Y-G. Early, but not late treatment with human umbilical cord blood-derived mesenchymal stem cells attenuates cisplatin nephrotoxicity through immunomodulation. *American Journal of Physiology Renal Physiology* 2016; 313(4): F984–F996.
60. Rivera-Cruz CM, Shearer JJ, Neto MF and Figueiredo ML. The Immunomodulatory Effects of Mesenchymal Stem Cell Polarization within the Tumor Microenvironment *Niche Stem Cells Int.* 2017; Article ID 4015039: 1-17.
61. Zhang F, Wang C, Wen X, Chen Y, Mao R, Cui D, Li L, Liu J, Chen Y, Cheng J and Lu Y. Mesenchymal stem cells alleviate rat diabetic nephropathy by suppressing CD103+ DCs-mediated CD8+ T cell responses. *J Cell Mol Med.* 2020; 24(10): 5817–5831.

## المخلص العربي

اثر الخلايا الجذعية في الحد من التغيرات في قشرة الكلى في الجرذ الناجمة عن مرض السكري :  
دراسة هستولوجية ، قياسية بينية و كيميائية حيوية .

حكمت احمد سرور ، منى محمد عبد الجليل

قسم الهستولوجيا - كلية طب (بنات) - جامعة الازهر، القاهرة، مصر

**الخلفية:** اعتلال الكلية السكري (DN) هو أكثر المضاعفات خطورة في مرض السكري. يعد العلاج بالخلايا الجذعية (MSCs) علاجاً واعداً ممتازاً في إصلاح الأنسجة والأعضاء المصابة. ومع ذلك ، لا تزال الآثار الدقيقة للخلايا الجذعية على الإصابة الخلوية الكلوية غير واضحة.

**الهدف من البحث:** تهدف هذه الدراسة الى تقييم الدور العلاجي المحتمل للخلايا الجذعية المشتقة من النخاع العظمي في تلف نسيج الكلى الناجمة عن اعتلال الكلى السكري المستحدث بعقار الستربتوزوتوسين في اناث الجرذان البيضاء البالغة.

**المواد والطرق:** تم تقسيم اناث الجرذان البيضاء البالغة إلى ثلاث مجموعات : المجموعة الأولى (المجموعة الضابطة) ، والمجموعة الثانية (مجموعة مرضى السكري) والمجموعة الثالثة (مجموعة مرضى السكري المعالجة بالخلايا الجذعية) حيث تم حقن  $1 \times 10^6$  من الخلايا الجذعية المميزة بأكسيد الحديد مرة واحدة في الوريد الموجود بذيل الفئران المصابة. تم تقدير مستويات الجلوكوز في الدم والتحليل الكيمائية الحيوية لوظائف الكلى مثل الكرياتينين (Cr) و نيتروجين اليوريا في الدم (BUN) وحمض البوليك . بعد ٨ أسابيع تم تحضير عينات الكلى لفحصها نسيجياً بالميكروسكوب الضوئي والالكتروني. كما أجريت القياسات المورفومترية والتحليلات الإحصائية.

**النتائج:** تسبب عقار الستربتوزوتوسين في حدوث تدهور في الحويصلات والانابيب الكلوية على هيئة تآكل بالخلايا المبطننة مع وجود فجوات بالسيتوبلازم ، وانوية ضامرة مع احتقان الشعيرات الدموية البينية وتسلل الخلايا الالتهابية والتي تآكدت بزيادة مستويات نيتروجين اليوريا و الكرياتينين وحمض اليوريك في الدم مقترنا ذلك بارتفاع كبير في تفاعل PAS مع زيادة كبيرة في النسبة المئوية من مساحة ألياف الكولاجين. وقد أكد التركيب النسيجي الدقيق هذه التشوهات. بينما أظهرت المجموعة المعالجة بالخلايا الجذعية تحسناً ملحوظاً في مستوى السكر بالدم والمعايير الكيمائية الحيوية لوظائف الكلى مع تحسناً كبيراً في التغيرات النسيجية الكلوية الموضحة سابقاً.

**الاستنتاج:** قد تلعب العلاجات القائمة على الخلايا الجذعية (MSC) دوراً علاجياً كبيراً في اعتلال الكلية السكري.